Title
Dynein Harnesses Active Fluctuations of Microtubules for Faster Movement

Author
Ezber, Yasin

Publication Date
2020

Peer reviewed|Thesis/dissertation

Dynein Harnesses Active Fluctuations of Microtubules for Faster Movement

By

Yasin Ezber

A dissertation submitted in partial satisfaction of the

requirements for the degree of

Doctor of Philosophy

in

Physics

in the

Graduate Division

of the

University of California, Berkeley

Committee in charge:

Professor Ahmet Yildiz, Chair
Professor Oskar Hallatschek
Professor Eva Nogales

Spring 2020

Abstract

Dynein Harnesses Active Fluctuations of Microtubules for Faster Movement

by

Yasin Ezber

Doctor of Philosophy in Physics

University of California, Berkeley

Professor Ahmet Yildiz, Chair

Motor proteins take part in the organization and division of eukaryotic cells by using their ability to move unidirectionally along the cytoskeletal tracks. While kinesin and myosin motor families have members that move towards either end of actin and microtubules, respectively, all dynein motors exclusively move towards the minus-end of microtubules. Previous studies reported that dynein asymmetrically responds to external forces, moving faster when pulled forward, while resisting backward movement under hindering forces. I hypothesized that this asymmetry enables dynein to harness energy from external force fluctuations for faster movement towards the minus-end.

In my doctoral work, I have shown that dynein can harness energy from cytoskeletal fluctuations. Using optical trapping techniques, I have characterized how external forces affect the velocity of dynein motility in the presence and absence of ATP. The results demonstrated that dynein forms an asymmetric slip bond with the microtubule. Using an oscillatory optical trapping assay, I showed that dynein can rectify force fluctuations to move towards the microtubule minus-end in the absence of ATP. Dynein was capable of moving towards the minus-end, even when the net force is in the plus-end direction. In the presence of ATP, dynein was able to move faster, generate power from force fluctuations, and stand against higher resistive forces. I developed a mathematical model that connects the force-induced release rate of dynein monomers with the force-velocity relationship of dynein dimers to describe dynein's reaction to force.

This dissertation is dedicated to my mom, Meryem Ezber, who has sacrificed all she has for her four children. She is the most patient person I know, and her unconditional love is the best gift I have received in my life. She will always be the person that I will seek the support of.

Acknowledgments

During my high school years, I feel the most privileged to have had the support of Prof. Recep Ventsislav Dimitrov, a Bulgarian Pomak Turk and a highly-regarded Physics Professor who prepared me for the International Physics Olympiads in Istanbul. His way of describing the physical concepts on a blackboard for hours at a time and our problem-solving sessions at 11 PM on weekdays were the most memorable. My close friend, Mustafa Sabih Kaya, who understood grad level physical concepts faster than anyone else, made these times so much more valuable.

Landing at UC Berkeley's Physics Department as an international Ph.D. student has widened my horizons. I realized there are many other skills to be learned to become a successful academic from my advisor Prof. Ahmet Yildiz. In Ahmet's lab, I have built upon my physics knowledge and sought help whenever I was in trouble. His immense support and guidance have enabled me to ask the right questions and make the right decisions. I thank my labmates: John Canty, Luke Ferro, Emre Kusakci, Amanda Jack, Andrew Hensley, Ruernsern Tan, Vladislav Belyy, Jigar Bandaria, Yavuz Selim Dagdas, Peiwu Qin, Sinan Can, Alexander Chien, Mohamed Elshenawy and Nicole Luk for making the lab a positive and supporting environment. I am especially grateful to Sinan Can who has helped me through hard days with his valuable friendship.

Many friends I have made in Berkeley were among the most valuable things during grad school. I am extremely grateful to Sara Tafoya and Itziar Ibarlucea Benitez who also helped me perfect my Spanish, and Atakan Köse, Burak Malkoç, Irene Guerra, Monica Hernandez and Alex Loera for their friendships. Thanks to our long coffee breaks and spontaneous barbeques, I always felt at home.

I am extremely grateful for my parents Cengiz and Meryem Ezber and my three beautiful sisters; Leyla Çaglar, Sare Özdemir, and Zeynep Deyan. They were always supportive despite their busy life. I especially thank my middle sister Sare, who always grabbed my hand and took care of me when I was a little kid.

TABLE OF CONTENTS

1. Introduction

Cytoskeletal Motors

Molecular motors play major roles in internal organization and coordination of eukaryotic cells. These motors harness the energy of ATP-hydrolysis to generate motion to carry intracellular cargos along the linear tracks. They bind to a cytoskeletal track in one end and to a cellular cargo on the other end and carry them over long distances by taking unidirectional steps along their respective track. Motors drive motility and force generation functions required for a wide range of cellular and developmental processes such as cell division, ciliary beating, and muscle contraction.

There are three different types of cytoskeletal motors: myosin, kinesin, and dynein. Myosin motors move along actin filaments, whereas dynein and kinesin move along microtubules (MTs)[1,2]. Dynein walks towards the minus-end of MTs, whereas most kinesins are plus-ended[3, 4].

The motility of cytoskeletal motors is driven by nucleotide-dependent conformational changes that act as a mechanical element[5]. These conformational changes are synchronized with nucleotide-dependent track binding and unbinding of the motor to take steps. Within an ATP hydrolysis cycle, an individual monomer of a typical cytoskeletal motor (1) binds strongly to its track, (2) produces a force-generating conformational change (powerstroke), (3) releases from its track, (4) performs a recovery stroke and (5) rebinds in a specific direction, resulting in unidirectional movement.

Myosin motors function along the actin filament. Myosin-II motors are not processive (an ability of a motor to take many successive steps before releasing from its track), and they need to work as a team to pull on the same actin filament for muscle contraction[6]. Myosin-V is a processive motor and a single myosin-V can carry cargo along the actin filaments[7]. While most myosins move towards the plus-end of actin filaments, myosin-VI moves towards the minus-end[1,2].

There are two types of motors acting along microtubules. Kinesin is similar to myosin in terms of its domain organization and mechanism. There are 15 subclasses of kinesins[8], which function as monomeric, dimeric, heterotrimeric, or tetrameric motors. While most kinesins are plus-end directed motors[4], kinesin-14s move towards the minus-end[9].

Dyneins are structurally distinct from kinesins and myosins and can be grouped into two categories; cytoplasmic and axonemal dyneins[3, 10]. Cytoplasmic dynein 1 heavy chain is the only dynein that functions in the cytoplasm of eukaryotic cells, and responsible for nearly all minus-end directed functions along MTs. It powers the transport of vesicles and organelles like endosomes[11], lysosomes[12], phagosomes[13], melanosomes[14], peroxisomes[15], mitochondria[16], lipid droplets[17], Golgi, mRNA[18] and even viruses[19] and transcription factors[20]. It also has major roles in cell division[21, 22], such as the movement of chromosomes and positioning the mitotic spindles for cell division by pulling on the MT network [23-25] and focusing the minus ends of MTs into the

poles [26-28]. Dynein plays crucial roles in neurons, because these cells are highly asymmetric and rely heavily on long-range transport. Cytoplasmic dynein takes part in synapse formation[29], neuronal migration[30], growth[31], and it powers retrograde transport towards the cell body[3, 32]. A malfunction of dynein motility is attributed to degeneration[33] and sensory neuropathy[34] in motor neurons, ALS[35], Alzheimer's disease[36], lissencephaly[37, 38], and schizophrenia[39]. Dynein 2, also known as intraflagellar transport (IFT) dynein, is closely related to cytoplasmic dynein 1 but its role is restricted to cargo transport from the tip to the base of cilia[40]. Axonemal dyneins are positioned between doublet MTs of an axoneme. They slide MTs relative to each other and power ciliary beating[41].

Because in my research I have focused on force production properties of cytoplasmic dynein (referred to as dynein hereafter), the following section will dive into more details about this motor.

Cytoplasmic Dynein

Dynein Structure and Mechanochemical Cycle

Dynein is a divergent branch of AAA ATPases[3]. Cytoplasmic dynein, which has a molecular mass of about 1.5 megadaltons (MDa), contains two identical 520 kDa heavy chains with the intermediate and light intermediate chains[42].

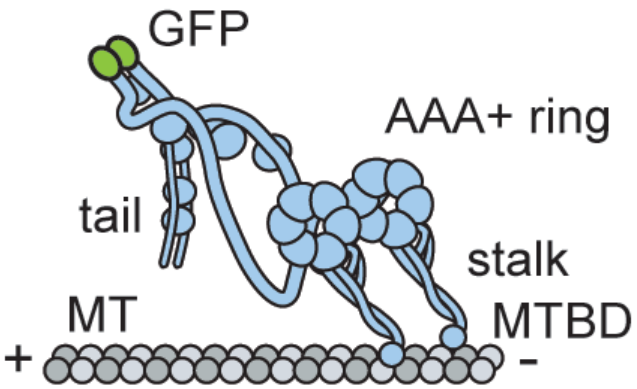

Figure 1. Dynein structure. *A GFP dimerized mammalian dynein is depicted. Motor domain (AAA+ ring) is connected to MT binding domain (MTBD) through a 10 nm coiled-coil stalk. Linker domain lies on the motor domain and extends to a tail domain where cargo binding happens.*

The C-terminal motor domain of the heavy chain is the core of the dynein transport machinery. Like other AAA enzymes, the dynein motor domain is a ring of six AAA subunits. In contrast to other AAA proteins, all AAA subunits are concentrated into a single polypeptide chain. AAA1-4 can bind ATP with AAA1 being the most critical and AAA3[43-45] acting like a switch by regulating the dynein motility and force generation[5, 46]. Remaining AAA5-6 have structural roles

for the appropriate conformational changes to happen. The motor domain connects to an MT through the stalk, an antiparallel coiled-coil that extends from AAA4/5 to a globular MT binding domain at the tip (Figure 1). The linker domain, an alpha-helical bundle that resides at the surface of the ring, undergoes ATP driven conformational changes to generate a powerstroke and forward movement. The registry of the stalk coiled coils also shifts in response to the nucleotide state of the AAA1 site, which enables the motor to release from the MT before it moves forward and rebinds the MT. The details of the mechanochemical cycle of a dynein monomer are illustrated in Figure 2.

The N-terminal tail domain of dynein is responsible for dimerization, cargo binding as well as the binding of regulatory light chains[47-49]. The tail domain also contains a light intermediate chain (LIC) and an intermediate chain (IC) which forms a complex with three other light chains (LCs) [10, 50, 51].

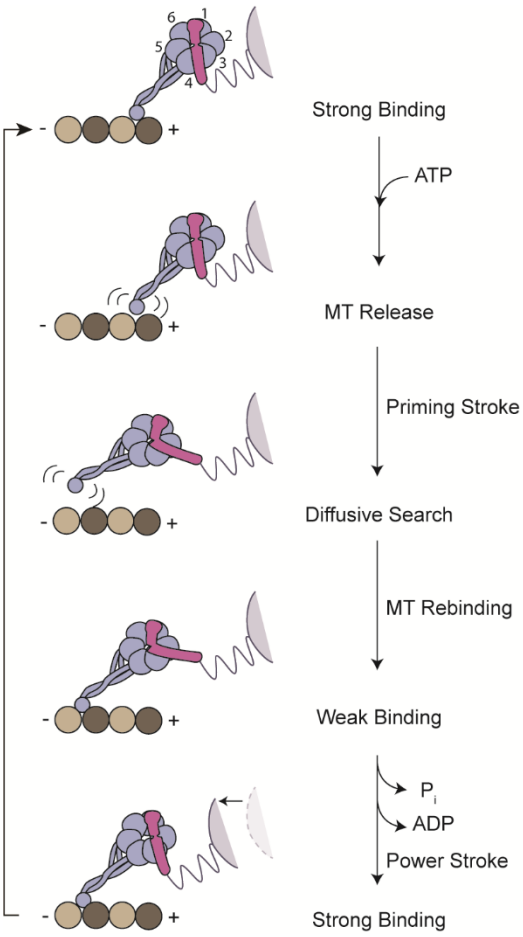

Figure 2. Mechanochemical cycle of a dynein monomer. *Dynein's stalk is tilted towards the plus-end at the base. AAA1 (where the linker emerges from) is the main catalytic site. Next 5 subunits are named similarly from AAA2 to AAA6 in a clockwise manner. In the absence of nucleotide, the protein is tightly-bound to MT with its linker lying on AAA4 in a straight orientation. When ATP binds to AAA1 domain[52], a conformational change is induced and translated through the coiled-coil in the form of a registry shift[46, 53], and the motor releases from the track. This is where the linker goes through priming stroke[48, 49, 54]. As illustrated in the 3rd step, the linker now lies on top of AAA2 and is aligned with the MT. This is where the MTBD moves towards the minus-end. With the hydrolysis of ATP, the motor rebinds to MT and releases the inorganic phosphate (Pi). In the ADP-bound state, the linker goes through a force-generating power stroke by realigning itself[48, 49, 54, 55]. With the release of ADP, dynein returns to its tightly-bound state and is ready for another cycle.*

I have studied cytoplasmic dynein from *S. cerevisiae* (budding yeast) and mammals. Dynein does not transport cargos in yeast cells and only has a nonessential role in the segregation of nuclei during cell division. In vitro studies have shown that yeast dynein heavy chain is a constitutively

active motor that moves processively in the absence of its cofactors and regulatory chains. In comparison, mammalian dynein heavy chain is auto-inhibited if it is not transporting cargos, and activation of its motility requires its association with dynactin and a cargo adaptor protein (referred to as dynein transport machinery). The formation of the dynein transport machinery is strongly favored by regulatory proteins, such as Lis1[56-58]. Cargo adaptors, such as BICDR, BICD2, Hook3 and TRAK1-2, contain a long coiled-coil region that links the tail of the heavy chain to the actin-like filament of dynactin. These proteins link dynein to specific vesicles for cargo transport or to the membrane for cell division[59-62].

Dynein Processivity and Stepping Pattern

Dynein processivity requires dimerization of the heavy chains. Single monomers would diffuse away from the MT after hydrolyzing a single ATP, evident from the mechanochemical cycle shown in Figure 2[63-65]. In vitro studies have demonstrated that the linker swing mechanism is also essential for *S. cerevisiae* dynein's processivity. When the monomers are immobilized to surface through C-terminus, they weren't able to glide MTs. ATPase mutations at the main catalytic site AAA1 and the connections between the linker and the surface of the ring also hinder the motility. However, artificial dimerization of dynein at the tail region results in robust motility, similar to full-length dynein.[46, 65]

The velocity of dynein depends on the species. Yeast cytoplasmic dynein is the slowest among the family with a velocity of 120 nm/s[39]. This can be compared to much faster other species where dynein moves at 1-3 μm/s[64, 66-69]. It is not entirely understood why the speed varies greatly among species, but this may have to do with MT affinity and ADP release rates of the motors from the MTs.

Dynein has a variable step size of 8-16 nm which corresponds to the distance between one to two heterodimers on a protofilament[39, 70]. Dynein takes frequent back steps and side steps, indicating that the third step of the mechanochemical cycle described in Figure 2 yields to a large diffusional component[65, 71]. This is in contrast to kinesin, which is forced to take consistent 8 nm steps because kinesin is drastically less flexible due to its short neck-linker between the heads[72-75]. The variable step size of dynein can be attributed to its flexibility in the motor domain. Dynein's step size is independent of ATP concentration and each step is generated by a single ATP hydrolysis [63, 70, 76]. Unlike kinesin, the stepping movement of dynein monomers is not strictly coordinated and either monomer can bind ATP and take a step. Besides ATP driven steps, dynein monomers can presumably take steps by minimizing the elastic strain energy stored in the linker[77].

Dynein also demonstrates bidirectional helical motility in MT bridge assays in three dimensions[78], compared to several members of kinesin and myosin family which rotate towards one direction exclusively[79, 80]. This specialty of dynein may enable it to avoid roadblocks more easily when carrying cargo, and in vitro studies demonstrated that dynein is more successful than kinesin to avoid obstacles along MTs.[81, 82]

Force Generation of Dynein

Dynein has a variety of functions in the cell such as carrying large intracellular cargos and mitotic spindle positioning that require this motor to withstand large forces. Single beam optical trap assays have been used to characterize the force generation of single dynein. These assays make use of micron-sized beads that are sparsely coated with motors. When the beads are trapped with a laser beam and brought right above an MT, the motor carries the bead along the MT. If the trap position is fixed, the motor experiences higher resistive forces as the bead moves away from the trap center. Eventually, the motility stalls because the resistive force exceeds the maximum force that can be generated by a single motor. The motor eventually releases from the MT and the bead snaps back to the trap center. This "stall force" is used to define the amount of maximum force that can be generated by a single dynein dimer. In vitro studies showed that single yeast dynein stalls at 3.4 pN force[70, 83, 84]. Dynein can stall for an extended amount of time on an MT, compared to kinesin which releases prematurely and more frequently[83-85].

Another way to utilize optical tweezers for force measurement is to use a force-clamp technique, where the trap "stalks" the bead movement at a certain distance. This enables the measurement of motor movement under constant forces. Previous work showed that the size and direction of dynein stepping can be altered by the magnitude and direction of external forces. Dynein is forced to step towards the plus-end under large forces both in the absence and presence of ATP. Remarkably, dynein moves faster when pulled towards the minus-end whereas it resists backward movement when pulled towards the plus-end.

DNA-tethered optical trap measurements have been performed to measure the force generation of a single head, showing that both heads of two monomers share the load and contribute equally to the force production[86]. Therefore, dynein monomers can be imagined to be elastically linked to each other, contrary to kinesin where one head handles the load[83]. Furthermore, the majority of the force is generated in the MT-bound state, as claimed by the powerstroke model[54].

Compared to yeast, mammalian dynein stalls at approximately 2 pN force because it is not a constitutively active motor. Formation of the dynein transport machinery by the BICD2 adaptor increases the complex stall force to 4.3pN[68, 87, 88, 87].

Release Rate of Dynein Monomers

Application of force on a dynein monomer bound to an MT results in the release of the monomer from the MT; which is in contrast to a dimer which would walk progressively with its "two legs" before it detaches. In order to understand the complex mechanics of a dynein dimer under force, it is crucial to use the reductionist approach, and determine how quickly a single monomer disassociates from its track under force.

To measure the release rate of a monomer, a tail-truncated dynein motor domain is attached to a micron-sized polystyrene bead either through a DNA tether or a GFP-antibody linkage[77]. The beads are then moved back and forth between two positions above the MT track in a square wave pattern by controlling the position of the trap. If a monomer binds to an MT, the bead and trap are separated from each other because the bead gets stuck on an MT and cannot follow the trap. In this case, the trap exerts a constant force on the monomer whose magnitude depends on the bead-trap separation and the trap stiffness. The distribution of the MT residence times before release versus force can be fit to a single or double exponential decay. The decay constant(s) is defined as the release rate of a monomer at a given force. Because the motor can bind to many positions along the MT as the bead is oscillated, this experiment enables measurement of motor release rate over a large range of forces.

Other approaches have been also used to detect the rupture forces of proteins, where a bead is moved at a constant velocity on an MT[88]. When a motor binds to an MT, it experiences a linearly increasing force. This assay measures the forces at which the motor is ruptured from the MT. With theoretical models, the rupture force measurements are translated into force-dependent release rates[89]. This method remains to be a more indirect measurement of the release rate compared to the constant-load assay. Furthermore, motors are expected to experience constant forces, rather than linearly increasing forces, when carrying cargos inside the cell. Therefore, I used constant-force experiments, instead of constant-velocity experiments to measure monomer release rates.

Earlier studies on kinesin showed that the release rate of a kinesin monomer increases with force in both directions[90]. Unlike kinesin, the force-induced release of a dynein monomer was dependent strongly on which direction the motor is pulled relative to the MT. The release rate of dynein increases exponentially when the motor is pulled towards the MT minus-end, and release under the plus-end directed pull of the trap is significantly slower. However, there is no consensus on how the motor responds to backward forces. The constant velocity measurements suggested that dynein forms a slip-ideal[89] bond with the MT. In this case, the release rate increases slightly under low backward forces and becomes constant at high backward forces. Constant force studies proposed that dynein forms an ideal bond[83] where the release rate stays constant independent of the backward force. In this case, the motor release was studied under low forces, and it remained unclear whether or not the release rate remains constant under low backward forces. Another study used inactive mammalian dynein heavy chain and proposed that this motor forms a catch bond[91], in which the release rate decreased under increasing backward load. This study needed to use a team of dimeric dynein motors in order for a bead to move processively. Therefore, how these results apply to a single dynein monomer remaines unclear.

The asymmetric response of dynein has been proposed to play a role in determining the direction of dynein motility. More recent work showed that overall directionality is determined by the linker swing mechanism, not by asymmetric release[92]. However, I had theorized that dynein can benefit from this asymmetry, especially under force fluctuations of active microtubule networks in the cell[93]. My dissertation focuses on determining how a dynein monomer releases under a wide range of constant forces, how the velocity of a dynein dimer is affected by constant forces

in the presence and absence of nucleotide, and finally how force fluctuations affect the velocity of dynein motility.

Techniques

Fluorescence Imaging

Motor proteins are ideal for imaging them under a fluorescence microscope. In single molecule dilution levels, they can be observed individually walking along their molecular tracks. To image proteins, they are tagged with a small organic dye during purification and flown into a chamber where molecular tracks are already immobilized on the surface. Total internal reflection florescence (TIRF) microscopy is a common technique used for the high-resolution imaging of the proteins[94]. Moreover, with the invention of more stable dyes and more sensitive cameras, it has recently become easier to track proteins and maintain high signal-to-noise ratio.

Single particle tracking has been a critical part of my research as it reveals a lot of insights about the motor proteins such as their processivity, directionality, helicity, velocity, run length and dwell time. Diffraction limit becomes a limiting factor in single particle tracking. For visible light, particles which are smaller than about ~200 nm become diffraction limited due to the resolution $R = \lambda/2NA$ (as numerical apertures (NAs) of both the objective and the condenser should be as high as possible for precise imaging). This is one order of magnitude higher than the actual size of a motor.

The center of the diffraction limited spot observed in the single molecule levels belongs to a single motor protein and it can be detected rather precisely. A two-dimensional Gaussian fit can be used to predict the center of the spot. The error in the detection of the center decreases as $1/\sqrt{N}$ as N; the number of detected photons increases. The precision goes up to ~1 nm as the photon number reaches to $\sim 10^4$. For faster motors, the frame number per second may need to be increased for better tracking and this reduces the photons collected per frame, which limits the temporal resolution. One quick fix for this problem is to observe the motor in low ATP conditions, hence when moving more slowly.

Another way to use the fluorescence imaging to analyze the motor proteins is the MT gliding assay as shown in Figure 3. Here, the proteins are immobilized on the glass surface and can glide an MT. This approach may come in handier, for instance, if one quickly wants to check the motility of a monomeric dynein construct or to find the directionality of a motor with polarity marked MTs[92].

Finally, fluorescence imaging can be combined with optical trapping for purposes such as figuring out the polarity of the MTs for force measurement experiments under no ATP conditions.

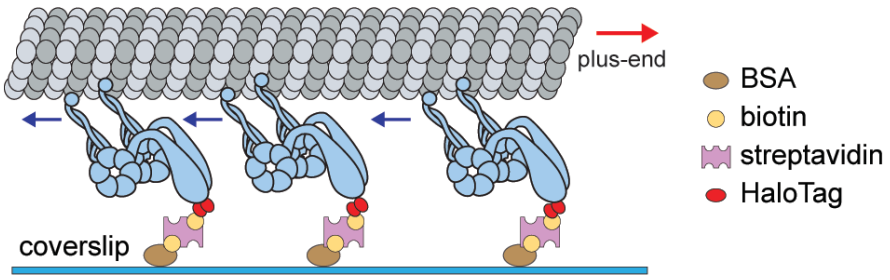

Figure 3. Gliding assay with dynein monomers. *This inverted geometry can be used for both monomers and dimers to test their ability to glide MTs. Here, the motors are fixed on the glass surface with a BSA-biotin-streptavidin linkage (a GFP-antibody linkage is also commonly used). Fluorescently labeled MTs can be observed under the microscope.*

Optical Trapping

Optical trapping has been a critical part of my research. It's important to know how motors function under tension to gain insight about their cellular functions. Inside the cell, motors carry large cargos and pull on MT networks and organelles for organization and cell division. With an optical trap, we can measure piconewton level forces and displacements in the nanometer scale with millisecond precision[95]. Application of force alters motors' velocity and stepping behavior and it can be used to understand how much force a single motor can withstand[65, 88]. Different geometries can be created using optical trap to analyze how a single motor reacts to a pull from its specific domains.

The idea behind optical trapping is rather simple. When a polystyrene bead comparable in size to the wavelength of the trapping laser beam is trapped, the beam travelling through the bead experiences a change in the momentum and creates a trapping force. Compared to this, if the bead is smaller compared to the wavelength, dipole effects need to be considered. The bead follows the trap as it moves and proteins that can be linked to beads with various linkages, are exerted force when they are bound to the molecular tracks. Within a short regimen, the bead-trap separation can be translated into force using the Hook's law: (± 150 nm is the linear regimen for our purposes) $F = -kx$. The trap stiffness is controlled by the laser power, the bead size and the viscosity of the environment (usually with glycerol).

There are many ways to use an optical trap. Figure 4a-b shows two techniques that Yildiz Lab has been using for a long time. The force-dependent release rate assay is advantageous to understand how quickly a monomer releases from its track under force. For motors that need to withstand large forces to perform its function, they need to have a smaller release rate. Moreover, an asymmetry in the release rate profile such as an increase in the release rate as force increases towards the minus-end and a different profile for the plus-ended releases, may give motors ratchet like properties. Indeed, this is exactly what happens in dynein's case.

For the release rate assay it's important to achieve single protein levels to understand the behavior of a single molecule as multiple proteins would often result in multiple releases from the track (compared to Figure 4a where a sharp/single release happens within Δt). This is achieved by making sure that more than 90% of the events result in a single release.

Fixed trap assay can be used to measure the stall force of a motor. In this scenario, the trap is held stationary and keeps exerting an increasing force as the motor walks away from the trap (Figure 4b). Maximum distance that the protein can walk is translated into the amount of force it can withstand. In comparison, force-feedback mode of a trap is used for application of directional force (usually along the MT long axis) on the motor. Here, the trap-bead separation is kept constant by a fast feedback such that the trap exerts a constant force on the protein. This method can be used to understand how load specifically affects the protein.

Another important method for my research was the oscillation technique where a motor can be exerted force periodically in a square wave manner in both direction as shown in Figure 4c. The net force can be biased in one of the directions. The net force can also be kept at 0 pN when the motor is pulled in both directions with the equal amount of force. One remarkable conclusion of my research is that in the absence of a net-force and ATP, dynein is able to harness energy from the force fluctuations to maintain its minus-ended directionality; hence extract power from the fluctuations and withstand larger forces.

Collective behavior of motor proteins can also be studied using optical trap. This can be achieved by using a DNA origami to tether multiple motors together or a geometry such as the one depicted in Figure 4d can be used. Furthermore, I combined the oscillation technique with Figure 4d to investigate the "ratchet-like" behavior of multiple dyneins together.

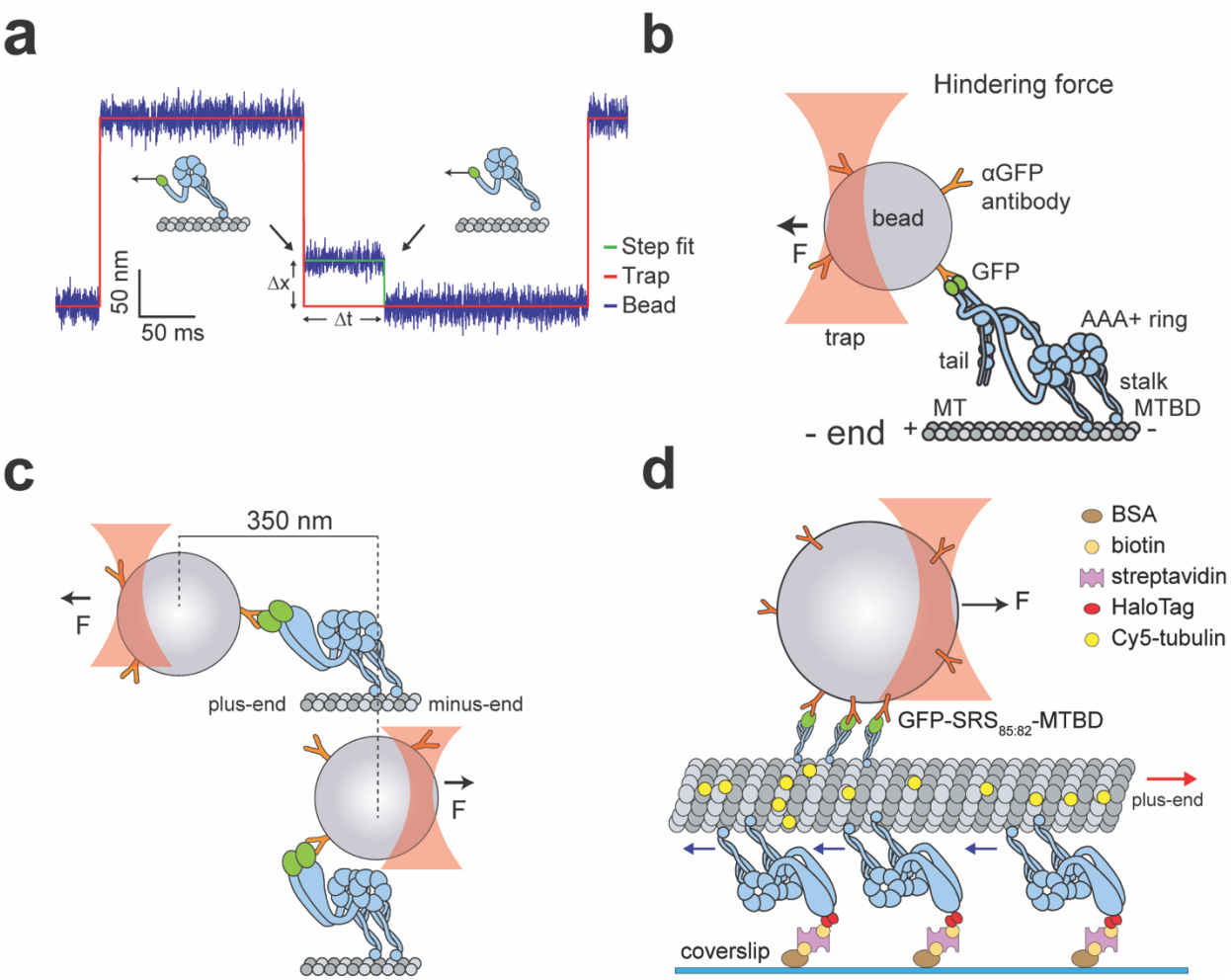

Figure 4. Various optical trapping techniques to analyze motor behavior. a. *Release rate of a yeast monomer is measured by collecting many data points as shown. Here Δt corresponds to the dwell time where the monomer feels force F = kΔx where Δx is the trap-bead separation and k is the trap stiffness constant.* ***b.*** *A human dynein (due to the existence of lights chains) is depicted under hindering force (towards MT plus-end). The connection to the polystyrene bead, which is typically more than 10 times larger than dynein, is established through a GFP-antibody linkage. Dynein can walk towards the plus-end in the presence of superstall forces.* ***c.*** *Creating "active fluctuations" for dynein using the optical trap. Depending on where the GFP connection happens, the bead can swing as much as 350 nm between two positions before the force is applied on dynein.* ***d.*** *A technique for the analysis of collective behavior of dyneins. The force is translated from trap to surface-immobilized dyneins first through a rigor GFP-SRS construct and then through the MT.*

2. Dynein Harnesses Active Fluctuations of Microtubules for Faster Movement

The work presented in this chapter was published in the following paper: Dynein harnesses active fluctuations of microtubules for faster movement written by Yasin Ezber, Vladislav Belyy, Sinan Can and Ahmet Yildiz**.** ***Nature Physics*** (2020)

Abstract

The cytoskeleton forms a dynamic network that generates fluctuations larger than thermal agitation of the cytoplasm[93]. Here, we tested whether dynein, a minus-end-directed microtubule (MT) motor[10], can harness energy from these fluctuations using optical trapping *in vitro*. We show that dynein forms an asymmetric slip bond with MTs, where its detachment rate increases more slowly under hindering forces than assisting forces. This asymmetry enables dynein to generate unidirectional motility towards the minus-end from force fluctuations. Consistent with our model, oscillatory forces exerted by the trap drive dynein stepping without net force and ATP. Dynein is capable of ratcheting towards the minus-end even when the net force is in the plus-end direction. With ATP, force oscillations increase the velocity and stall force of dynein as it transports cargos and glides MTs. Therefore, dynein is a mechanical ratchet that rectifies cytoskeletal fluctuations to move faster and resists higher forces along MTs.

Introduction

The cellular interior is highly dynamic and far from equilibrium[93]. Mechanical properties of the cytoplasm are dominated by dynamics of cytoskeletal filaments, MT and actin, which harness energy from nucleotide triphosphate hydrolysis. These polar filaments rapidly polymerize and depolymerize, providing a continuous supply of mechanical energy to the cell. Molecular motors (actin-associated myosins and MT-associated kinesins and dyneins) additionally use energy from ATP hydrolysis to generate force and mechanical work along these tracks. Collectively, the cytoskeleton forms an active network. Forces generated by filament polymerization and motors control the flow of cytoplasmic streaming and drive the motion of large objects in the cytoplasm[93, 96, 97]. Unlike thermal agitations, the energy of these fluctuations can in principle be harnessed by molecular machines to perform mechanical work.

While the roles of molecular motors in motility, contractility, and self-organization of cytoskeletal networks are studied in detail, little is known about how active fluctuations of cytoskeleton affect the mechanics and cellular function of cytoskeletal motors and non-motor proteins. MT-associated proteins (MAPs), such as NuMA and EB1, exhibit asymmetric friction when they crosslink a pair of actively moving MTs and this may be a viable strategy for these proteins to diffuse towards one end during MT growth and shrinkage[98]. Actin-binding proteins, vinculin, and cadherin-catenin form a force-dependent catch bond when pulled toward the pointed-end compared to the barbed-end. This directional and force-stabilized binding to F-actin was proposed to reinforce cell adhesion and maintain front-rear asymmetry in migrating cells[99,

[100]. Similarly, myosin II and kinesin-8 motors respond asymmetrically to the external force and diffuse at different speeds towards the plus- and minus-ends of actin and MT under load[101, 102].

It remains unclear whether processive motors can harness energy from cytoskeletal fluctuations for faster stepping along their tracks. Optical trapping studies revealed that dynein (Figure 6a), a motor protein responsible for nearly all motility and force generation functions towards the MT minus-end, rapidly releases from MTs and moves faster when pulled forward, while resisting backward movement when pulled towards the plus-end[77, 83, 84, 89]. This asymmetry has been proposed to play a role in interhead coordination of dynein motility[76, 77, 103], as well as tight anchoring of dynein to MT under high tension[91, 104].

Results

Dynein forms an asymmetric slip bond with microtubule

In order to test dynein's ability to harness energy from cytoskeletal fluctuations, we first characterized the force-dependent kinetics of the dynein-MT bond. Previous studies proposed that dynein-MT is a slip-ideal[89], ideal[83] or catch[91] bond, predicting that the release rate remains constant or decreases under high hindering forces (Figure 5a). These models could not be distinguished because of the small changes in the velocity and MT release rate of dynein under low (1-5 pN) hindering forces (Figure 5a). To address this, we measured the MT dwell time of single *S. cerevisiae* cytoplasmic dynein ("dynein" hereafter) monomers[65] under a wider range (1-14 pN) of forces using an optical trap[77, 90] (Figure 6b, Figure 7). The dwell time distributions fit well to a double exponential decay. MT release rate is interpreted as the slow rate of the fit, whereas the fast rate likely represents weak interactions between dynein and MT (Figure 5b-d). Consistent with previous studies[77, 89], we observed that the release rate rapidly increases when dynein is pulled toward the MT minus-end (assisting) and release is slow at low (1-4 pN) hindering forces in the absence of ATP. However, we clearly detected an increase in MT release rate at higher hindering forces (6-14 pN), albeit less drastically than release under the forward pull of the trap (Figure 5c). These results showed that dynein forms an asymmetric slip bond with an MT. Force-detachment kinetics of dynein from MT can be described by a model[102] based on the Arrhenius theory (see Theory). In the absence of force and nucleotide, forward (k_{minus}) and backward (k_{plus}) release rates are equal:

$$(1)\ k_{minus} = k_{plus} = k_0^{apo} \propto e^{-\Delta G_0/k_B T}$$

where k_0^{apo} is the release rate and ΔG_0 is the energy barrier in the absence of force and nucleotide, k_B is the Boltzmann constant and T is the absolute temperature (Figure 5d, i). An external force (F, positive forces are in the plus-end direction) biases the potential landscape and increases the release rate towards the direction motor is pulled from the MT (Figure 5d, ii).

$$(2)\ k_{minus} = k_0^{apo} e^{-F(\frac{\delta}{2}+A)/k_BT},\ k_{plus} = k_0^{apo} e^{F(\frac{\delta}{2}-A)/k_BT}$$

where *A* is the asymmetric distance that biases the energy barrier for the release from the MT, and δ is the barrier width (Figure 5d, i). The total release rate (k_{total}) is given by:

$$(3)\ k_{total} = k_{minus} + k_{plus} = 2k_0^{apo} e^{-\frac{F\,A}{k_BT}} cosh\left(\frac{F\delta}{2k_BT}\right)$$

The fit of force-dependent release rate to equation 3 reveals that *A* of dynein (0.73 ± 0.10 nm, Figure 5c) is higher than the previously reported values for kinesin-8[102], NuMA, and EB1[98], suggesting that dynein is a stronger ratchet than these proteins. We note that δ (3.4 ± 0.3 nm) represents the distance over which external force acts on a dynein monomer to release it from MT, and it is shorter than the distance between adjacent tubulin binding sites (8.2 nm). Due to the vertical forces inherent to the single bead trapping assay[105], we anticipate that k_0^{apo} of the motor is lower than 0.6 ± 0.1 s^{-1} we measured and dynein exhibits even greater asymmetry in the absence of vertical forces.

The faster release rate profile in Figure 5c is similar to the slower release rate profile but we speculate that as the resolution is increased, weaker interactions between the motor and the MT can be detected and an even faster third rate can be recorded. There is still an order of magnitude difference between the slow and fast rates so they can be easily distinguished from each other in both backward and forward directions (Figure 5d).

Forces as high as 15pN were applied in the backward direction to detect the release rate, as previously mentioned, this was necessary to distinguish the three suggested models for the release rate profile. Upon the concerns that the GFP-antibody linkage may not be strong enough to withstand such high loads, the force versus release profile of dynein monomer was repeated with a 74 bp long DNA. It connects to the motor through a C-terminal DHA tag and to the bead through a biotin-streptavidin linkage (Figure 7), and the release rate profile was found to be very similar to N-terminal GFP tether experiment where, most critically the release rate profile increased as moderately in the backward direction.

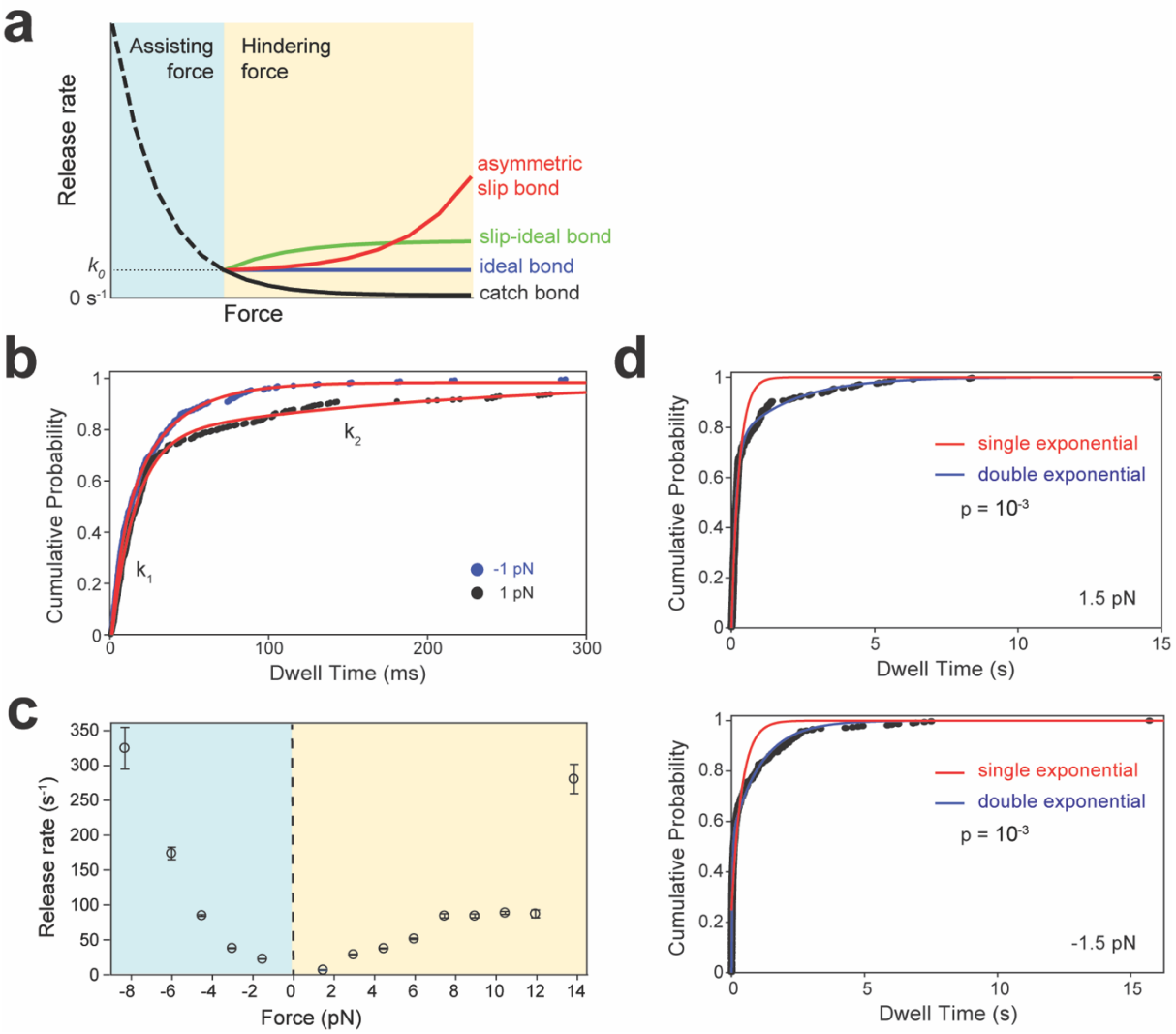

Figure 5. Force-induced release rate analysis of dynein. a. *When pulled towards the minus-end, dynein exhibits a slip bond behavior with an MT, in which the release rate increases exponentially by assisting force (black dashed curve). In the hindering direction, possible force-detachment kinetics of slip, slip-ideal, ideal and catch bond behavior are shown for comparison (solid curves).* ***b.*** *Cumulative distributions of dynein dwell time on an MT under a given force were fit to a double exponential decay (red curves) to calculate fast (k_1) and slow (k_2) release rates from MT. n = 504 for 1 pN and 512 for -1 pN.* ***c.*** *k_1 of dynein from MT (mean ± s.e.m.; n = 270, 243, 479, 407, 385, 354, 487, 461, 380, 260, 208, 325, 137, 325 from left to right). This rate likely represents a weak interaction between dynein and tubulin. Similar to k_2 (Figure 6c), k_1 increases with force in both directions.* ***d.*** *Comparison of the single and double exponential fit to example cumulative distributions of dynein dwell time. p values are calculated using F-test.*

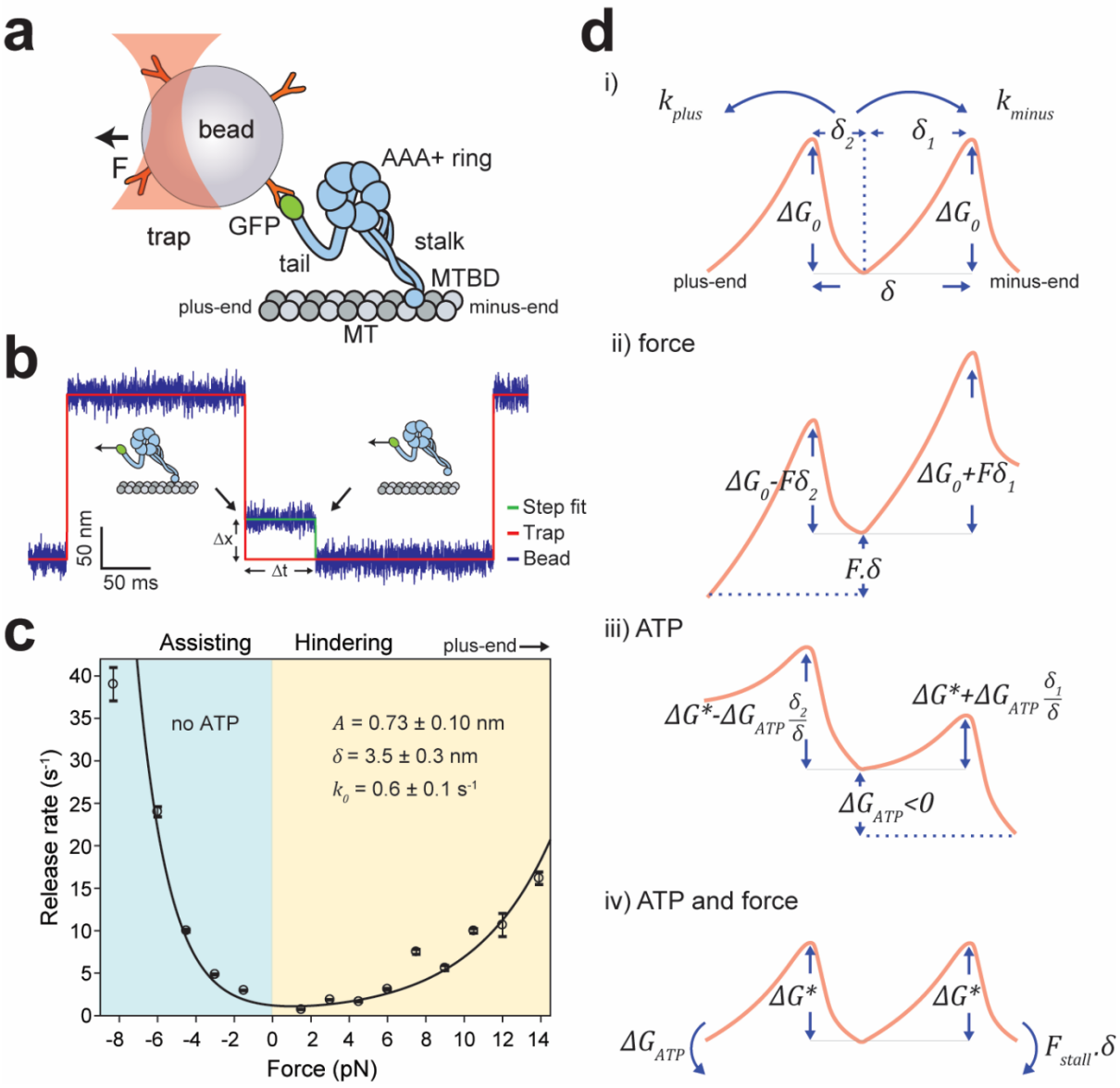

Figure 6. Dynein forms an asymmetric slip bond with an MT. a. *Schematic of a dynein motor domain. Dynein heavy chain has a catalytic AAA+ ring, which connects to an MT through a coiled-coil stalk. Dynein was attached to an 860 nm-diameter polystyrene bead from its tail using the GFP-antibody linkage and trapped with a focused laser beam (not to scale).* ***b.*** *Measuring the force-induced release of dynein monomers from MTs. (Inset) A trapped bead coated with monomeric dynein is oscillated between two positions 200 nm apart. When a dynein monomer binds to the MT, the bead does not follow the trap to its next position (black arrows). A constant force is applied due to trap-bead separation (Δx) until dynein releases from MT (Δt).* ***c.*** *The release rates of dynein monomers from MT under force are calculated from an exponential decay fit to the dwell-time histograms (± s.e.; n = 270, 243, 479, 407, 385, 354, 487, 461, 380, 260, 208, 325, 137, 325 from left to right, see Figure 5). The solid curve represents a fit to equation 3. Errors in derived parameters are s.e. of the fit.* ***d.*** *The model for the asymmetric potential landscape of dynein along an MT in the presence and absence of a nucleotide and external force* $(\delta_{1,2} = \delta/2 \pm A)$*. The energy barrier in the presence of ATP* (ΔG^*) *is lower than the*

apo condition (ΔG_0). Work done by hindering force ($F\delta$) shears the energy landscape towards the plus-end (ii), while the free energy of ATP hydrolysis (ΔG_{ATP}) shears it towards the minus-end (iii). At $F_{stall} = -\Delta G_{ATP} / \delta$, the motor comes to a stall because the negative work done by hindering force is equal to the positive work done by ATP hydrolysis (iv).

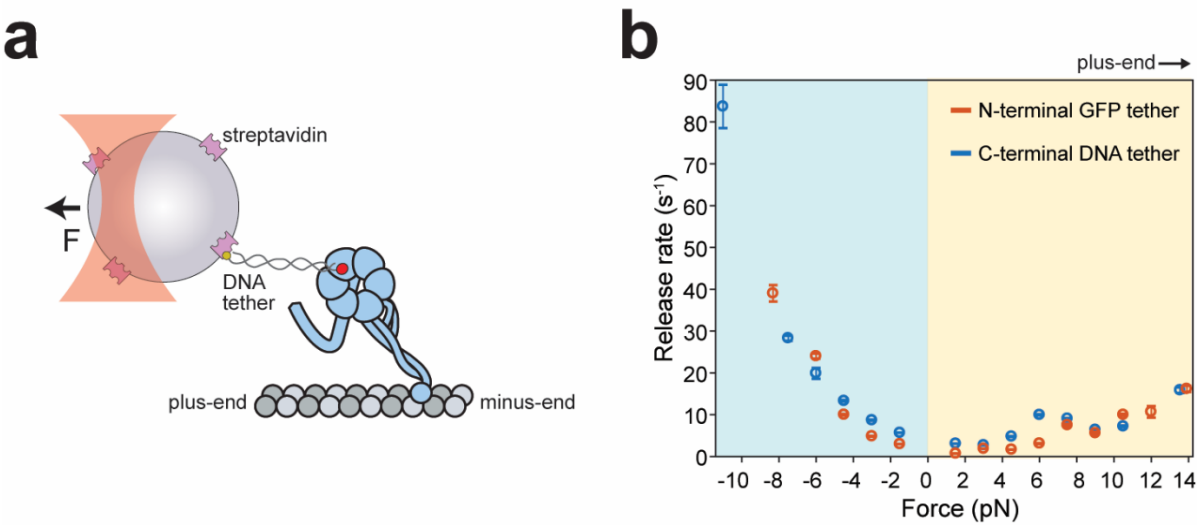

Figure 7. Measurement of force-detachment kinetics of dynein using a DNA-tethered optical trap. a. *A tail truncated dynein monomer (GFP-Dyn$_{331kD}$-DHA) was labeled a 74 bp DNA tether at its C-terminal DHA tag using the HaloTag chemistry. The DNA-labeled motor was attached to a bead via a biotin-streptavidin linkage.* ***b.*** *MT release rates of dynein monomers pulled from the C-terminal AAA ring via a DNA tether (blue, mean ± s.e.m.; from left to right n = 534, 661, 251, 973, 1074, 1742, 3216, 1423, 1003, 984, 792, 501, 310, 240 from three technical replicates). MT release rates of dynein monomers pulled from the N-terminal linker via the GFP-antibody (red, Figure 1c) are shown for comparison.*

Dynein responds asymmetrically to assisting and hindering loads

To determine how force affects the velocity of dynein dimers, we applied constant forces to beads transported by single full-length dynein[65] (Figure 7a). In the absence of ATP, dynein was immobile without force and moved processively towards the direction it was being pulled by the optical trap[84]. Consistent with its asymmetric force-dependent detachment from MT, dynein moved faster towards the minus-end compared to the plus-end under the same magnitude of force (Figure 8b)[83, 84, 92].

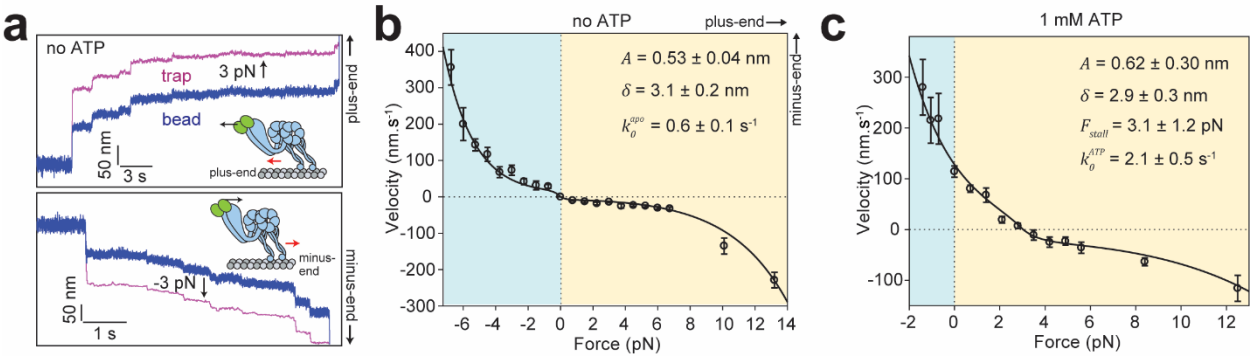

Figure 8. Dynein responds asymmetrically to assisting and hindering forces. a. *Representative position-time graph of a dynein motor under constant 3 pN hindering (top) and assisting (bottom) force. (Insets) Dynein moves (red arrows) towards the direction of the applied force (black arrow).* ***b.*** *F-V relationship of dynein in the absence of ATP (mean ± s.e.m.; from left to right n = 51, 50, 59, 53, 41, 35, 48, 46, 43, 54, 62, 47, 82, 68, 56, 92, 85, 44, 45, 78 from 3 technical replicates).* ***c.*** *F-V relationship of dynein in 1 mM ATP (mean ± s.e.m.; from left to right n = 38, 36, 48, 78, 42, 56, 58, 47, 39, 35, 35, 48, 43, 42 from three technical replicates). In b and c, the solid curves represent a fit to equations 3 and 5, respectively (see Theory). Errors of the derived parameters are s.e. of the fit.*

The average velocity (*V,* positive velocities are in the minus-end direction) at a given force is given by:

$$(4)\ V(F) = k_{total}(F)d(F)$$

where $d(F)$ is the average step size of dynein in the absence of ATP, measured from the step analysis of individual trajectories under constant load (Figure 9). The fit of experimentally measured $V(F)/d(F)$ values to equation 3 (Figure 9d) revealed similar k_0^{apo}, A and δ values estimated from the force-dependent release rates of monomeric dynein (Figure 5c). Note that even though there is no motility due to ATP application of force in either direction results in motor taking steps in both directions. This is because of the diffusional search that each head goes through once it releases from the MT.

Figure 9c reveals the step ratios under a constant force pull. For a plus-ended pull, the majority of the steps are towards the plus-end, and the same is valid for a minus-ended pull. As the force increases in one direction, the ratio of the steps in that direction also increases (Figure 9b). We have interpolated the step size values with a sharply increasing exponential function to use it to calculate the release rates based on the velocities.

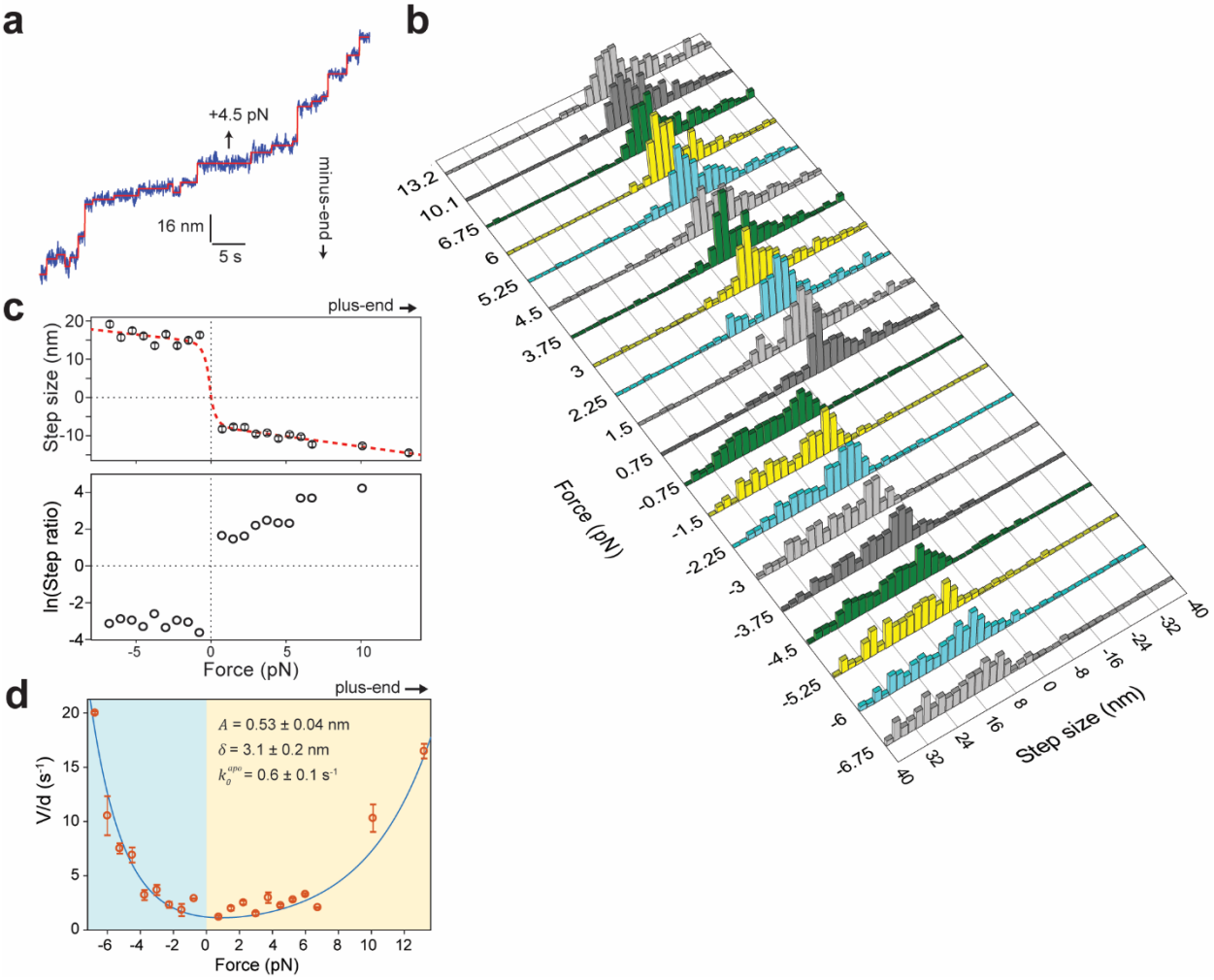

Figure 9. Force-induced stepping of dynein in the absence of ATP a. *Example trajectory of a bead driven by single full-length dynein at 4.5 pN hindering force (blue) in the absence of ATP. Red horizontal lines represent a fit with a step finding algorithm (see Methods).* ***b.*** *Step size distribution of dynein under assisting and hindering forces in the absence of ATP (n = 214, 207, 204, 203, 266, 316, 308, 400, 211, 233, 247, 233, 202, 204, 238, 205, 226, 203, 208, 265 steps from hindering to assisting forces).* ***c.*** *(Top) The average step size of dynein under different forces. Positive steps are in the minus-end direction. Error bars represent s.e.m. The red dashed curve is an interpolation of the data to an exponential function. (Bottom) The ratio of steps taken in the plus-end direction to minus-end-direction.* ***d.*** *The ratio of the experimentally measured velocities (Figure 8b) to the average step size (c) in the absence of ATP. The errors represent s.e.m. of velocity measurements (Figure 8b). The blue curve represents a fit to equation 3. The errors of the derived parameters are s.e. of the fit.*

We next determined how force affects dynein velocity in saturating (1 mM) ATP. Similar to Gennerich et al.[84], we observed that dynein asymmetrically responds to load, and moves processively backward under high resistive forces (Figure 8c)[83, 84]. However, we observed dynein to move at higher velocities (114 ± 11 nm s^{-1}, ± s.e.m.) in unloaded conditions[65] and the

velocity increased rapidly under forward load. In addition, we did not see evidence of a nonadvancing stepping mode[84], in which the motor takes consecutive forward and backward steps at the same position on an MT under load. These disparities may be related to differences in assay conditions and calibration of the force response of the optical trap.

To determine how energy from nucleotide hydrolysis biases the potential landscape towards the minus-end (Figure 6d, iii), we fit the F-V measurements to:

$$(5)\ V(F) = 2d(F)k_0^{ATP} e^{-\frac{(F-F_{stall})\,A}{k_B T}} cosh\left(\frac{(F-F_{stall})\delta}{2k_B T}\right)$$

where k_0^{ATP} is the release rate in the absence of force, and F_{stall} is the hindering force at which $k_{minus} = k_{plus}$ (Figure 6d, iv). The average step size in ATP at a given force $(d(F))$ is measured from individual trajectories under constant load (Figure 10). The fit revealed similar *A* and δ values to the no nucleotide condition (Figure 10 d). F_{stall} (3.1 pN) is consistent with earlier measurements in fixed trap assays[83] and lower than 7 pN stall force reported by Gennerich et al[84] (Figure 8c). Notably, k_0^{ATP} is ~4 fold higher than k_0^{apo}, which might result from switching of dynein from strongly-bound to weakly-bound states during the nucleotide hydrolysis cycle.

Dynein takes steps in both directions in the presence of ATP and under force. The average step-size of dynein approaches to 0 nm around 3.1 pN which is defined as F_{stall} where, dynein produces the maximum force. The force towards the MT minus-end biases the step size distribution more easily compared to the plus-ended forces. This is because dynein is more prone to release towards the minus-end during the diffusional search in the presence of ATP.

The average step size values in Figure 10c are similarly interpolated using a sharply increasing exponential function to calculate the release rates (Figure 10d) using the force-velocity curve under saturating ATP conditions.

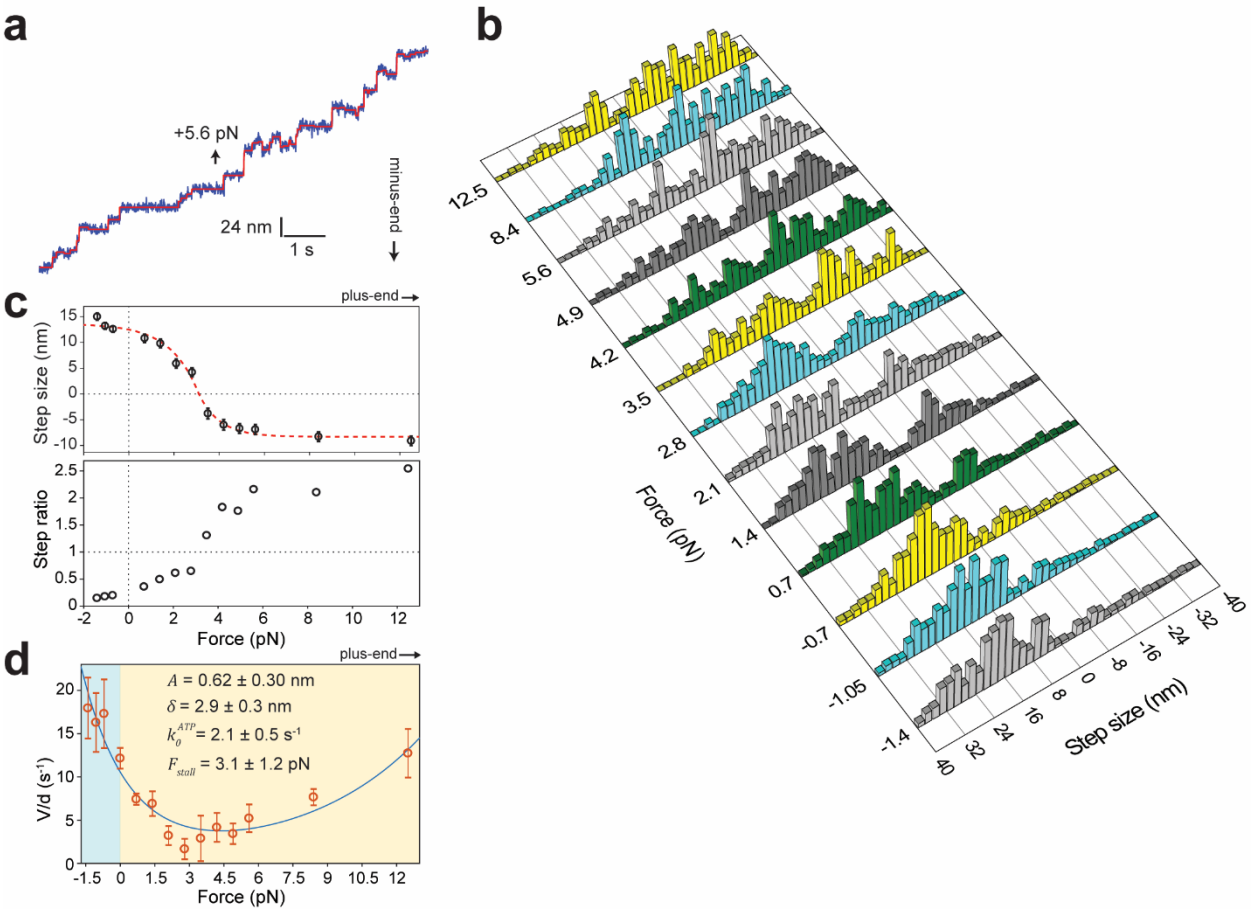

Figure 10. Force-induced stepping of dynein in 1 mM ATP. a. *Example trajectory of a bead driven by single full-length dynein at 5.6 pN hindering force (blue). Red horizontal lines represent a fit with a step finding algorithm.* ***b.*** *Step size distribution of dynein under assisting and hindering forces (n = 447, 428, 492, 430, 440, 460, 442, 291, 314, 381, 335, 298, 340 steps from hindering to assisting forces).* ***c.*** *(Top) The average step size of dynein under different forces. Error bars represent s.e.m. The red dashed curve is an interpolation of the data to an exponential function. (Bottom) The ratio of steps taken in the plus-end direction to minus-end-direction.* ***d.*** *The ratio of the experimentally measured velocities (Figure 8c) to the average step sizes (c) in 1 mM ATP. The errors represent s.e.m. of velocity measurements (Figure 8c). The blue curve represents a fit to equation 5. The errors of the derived parameters are s.e. of the fit.*

Force oscillations drive minus-end-directed motility of dynein without ATP

To test whether this asymmetric F-V relationship enables dynein to harness energy from cytoskeletal oscillations, we designed an experiment analogous to Feynman's hypothetical "ratchet and pawl" device[106], in which a microscopic ratchet generates work from random fluctuations that occur at an effective temperature higher than the ambient temperature (Figure 11a). We increased the effective temperature, but not the actual temperature, of a single dynein's local environment by oscillating the optically trapped bead (Figure 11b-c). We first checked whether force fluctuations can drive unidirectional motility without ATP and the net force on the bead ($\bar{F} = (F_{plus} + F_{minus})/2$). The magnitude of force oscillations ($\Delta F = F_{plus} - F_{minus}$) was increased from 0 pN to 13 pN, while $\bar{F}$ was kept at 0 pN (Figure 11d-e, Figure 12).

Consistent with our prediction, dynein processively moved towards the minus-end when subjected to force oscillations in a square wave pattern and the velocity increased with ΔF (Figure 11e). This is significant because dynein is able to generate power and withstand higher resistive forces in the presence of force fluctuations with 0pN net force (Figure 11c). The ΔF-V relationship is consistent with the average velocities of dynein under F_{plus} and F_{minus} (Figure 8b and 11e).

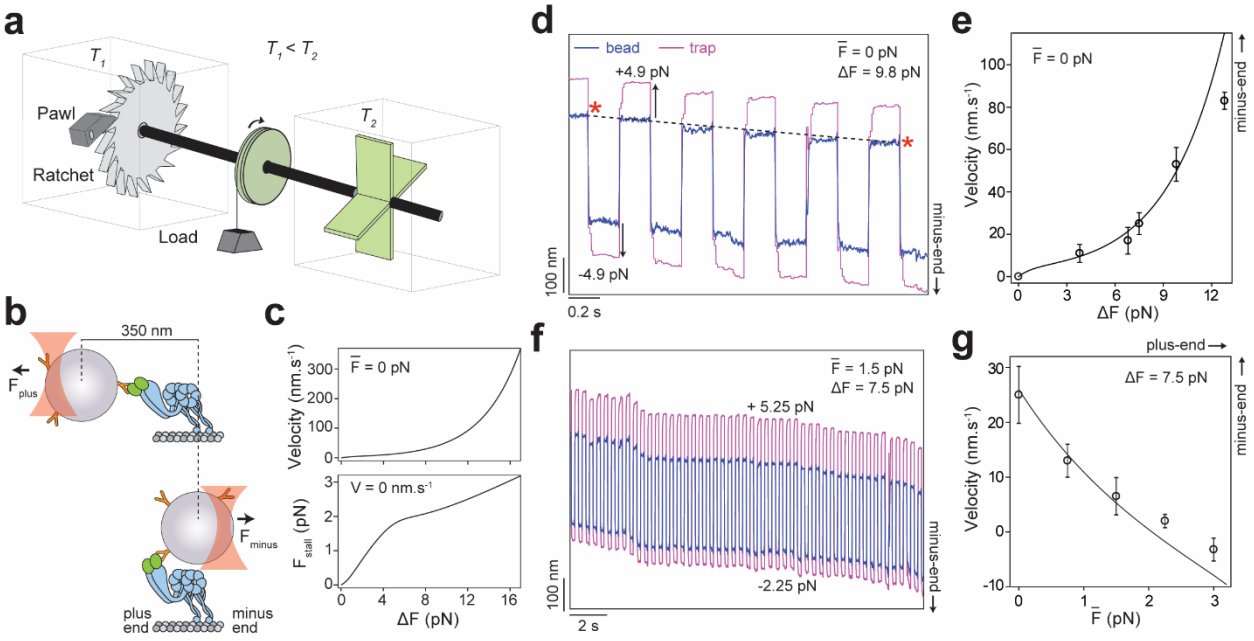

Figure 11. Force oscillations drive minus-end-directed motility of dynein without ATP. a. *Feynman's microscopic ratchet device. Two chambers are maintained at temperatures T_1 and T_2. Thermal fluctuations in the right chamber drive the shaft. The ratchet generates net clockwise rotation and lifts the load if $T_2 > T_1$.* ***b.*** *Dynein is driven by back-and-forth oscillations of the optically trapped bead, which increase the local effective temperature above that of the environment. Due to the rotational freedom of the bead, the trap freely moves 350 nm between the assisting and hindering directions before applying a*

significant force on dynein. ***c.*** *The estimated velocity and stall force of dynein under force oscillations are calculated from the F-V curve in Figure 8b.* ***d.*** *A dynein-driven bead oscillated ±4.9 pN in a square wave pattern at 2.5 Hz exhibits motility towards the MT minus-end. Velocity is calculated from the ratio of the net displacement of the bead (black dashed line) to elapsed time (red stars).* ***e.*** *The minus-end-directed velocity of dynein-driven beads increases with ΔF (mean ± s.d.; from left to right n = 32, 35, 25, 39, 42 from three technical replicates).* ***f.*** *Example trajectory of a dynein-driven bead oscillated with 5.25 pN hindering and -2.25 pN assisting forces at 2.5 Hz.* ***g.*** *The velocity of dynein-driven beads decreases by the increase in the average hindering force on the bead (mean ±s.d.; from left to right n = 25, 23, 29, 28, 25 from three technical replicates). In d and f, black curves represent the estimated velocities from the F-V curve in Figure 8b.*

To test the effectiveness of dynein's ratcheting along MTs in the absence of ATP, we biased the net force $\bar{F}$ from 0 pN to 3 pN towards the plus-end while keeping ΔF constant (7.5 pN). Remarkably, dynein was able to move towards the minus-end even though it was pulled more strongly towards the plus-end. This proves that dynein is such a strong "ratchet" that it can withstand forces that are biased towards the plus-end and still maintain its minus-endedness to some extent. Even though the velocities in Figure 11g are comparable slow due to the averaging out of the velocities in both directions, this case can be used as a proof of principle to argue that dynein behaves as expected based on its force velocity curve (Figure 8)

Furthermore, in the presence of plus-ended bias, the motor stalled at $\bar{F} = 2\ pN$, and moved backward under higher hindering loads (Figure 11f-g, Figure 12).

An important challenge in calculating the velocities in the presence of force-fluctuations can be visualized in Figure 12 where, in some rare cases trap does not switch between two locations fast enough, which effectively decreases the amount of time the fluctuations are present. This is accounted for in the analysis of the data by correcting the total amount of time in calculation of the velocities. Figure 12c demonstrates two different cases where the dead time is considerably different.

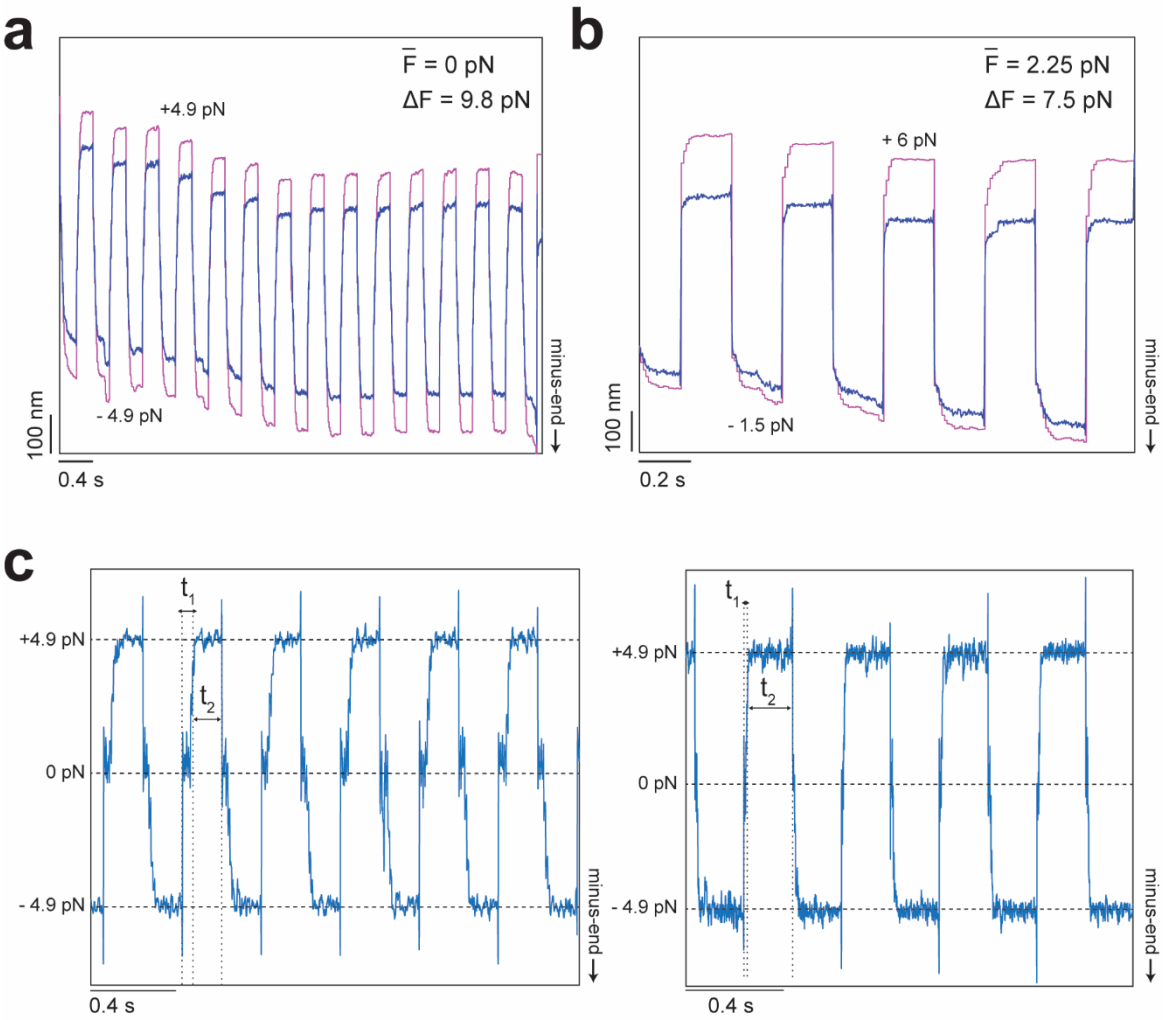

Figure 12. Example traces for nucleotide-free oscillations. a. *Example trajectory of a dynein-driven bead oscillated ±4.9 pN in a square wave pattern without ATP.* ***b.*** *Example trajectory of a dynein-driven bead oscillated with +6 pN and -1.5 pN in a square wave pattern at 2.5 Hz. Even though dynein was pulled more strongly backward, it moved towards the MT minus-end in the absence of ATP.* ***c.*** *The bead position was subtracted from the trap position to determine the force exerted on the bead during force oscillations. Due to the thermal relaxation of the bead and the rotational freedom of the bead-motor linkage, the bead-trap separation reaches near zero when the bead is moved between forward and backward positions. To determine how force affects velocity, this "dead" period t_1 is omitted from total elapsed time and t_2 is taken as half period of oscillations. (Left) To change force on the bead, the trap is first moved 250 nm and then with proportional feedback-controlled increments every 10 ms until the desired force is reached. (Right) The trap is first moved 500 nm and then with feedback-controlled increments every 10 ms until the desired force is reached. An increase in this "overshoot" distance decreases t_1.*

Force oscillations also facilitate ratcheting of mammalian dynein-dynactin

We started with yeast cytoplasmic dynein to study the ratchet-like behavior of dynein but it can be generalized to other species; most importantly mammalian dynein. Mammalian dynein is not constitutively active and requires the assembly of cofactors such as dynactin and a cargo adaptor to become motile, but it can still be recruited to the organelles without a cofactor[107, 108]. Unlike mammalian dynein, yeast cytoplasmic dynein is constitutively active even in the absence of dynactin and a cargo adaptor and exhibits robust motility *in vitro*. It has been assumed that the yeast dynein is an exception as it does not transport cargos. Recent studies successfully reconstituted mammalian dynein and a cofactor and started to alter the views[68, 69, 109]. These studies found that mammalian dynein is auto-inhibited when not transporting cargo. Yet, when dynein forms a complex with dynaction and a cargo adaptor, it moves rapidly along MTs[68, 69] and produces high forces[87].

Recent studies have been published around stepping and force generation of mammalian dynein-dynactin complexes. They have showed that once activated, mammalian dynein-dynactin has a similar stepping behavior, stall force and a force-velocity relationship to yeast dynein[61].

We have repeated some conditions with mammalian dynein and observed the mammalian dynein-dynactin-BicD2N (DDB) complex[87] to move processively towards the MT minus-end under force fluctuations in the absence of ATP and net force (Figure 13), suggesting that ratcheting is a general property of dynein motors.

We argue that the behavior seen in Figure 6 and 8 applies to mammalian dynein, too. One caveat of working with mammalian dynein in optical trap is its high velocity which is around 1-3 μm compared to an order of magnitude slower velocities with yeast cytoplasmic dynein[59, 61, 91, 110].

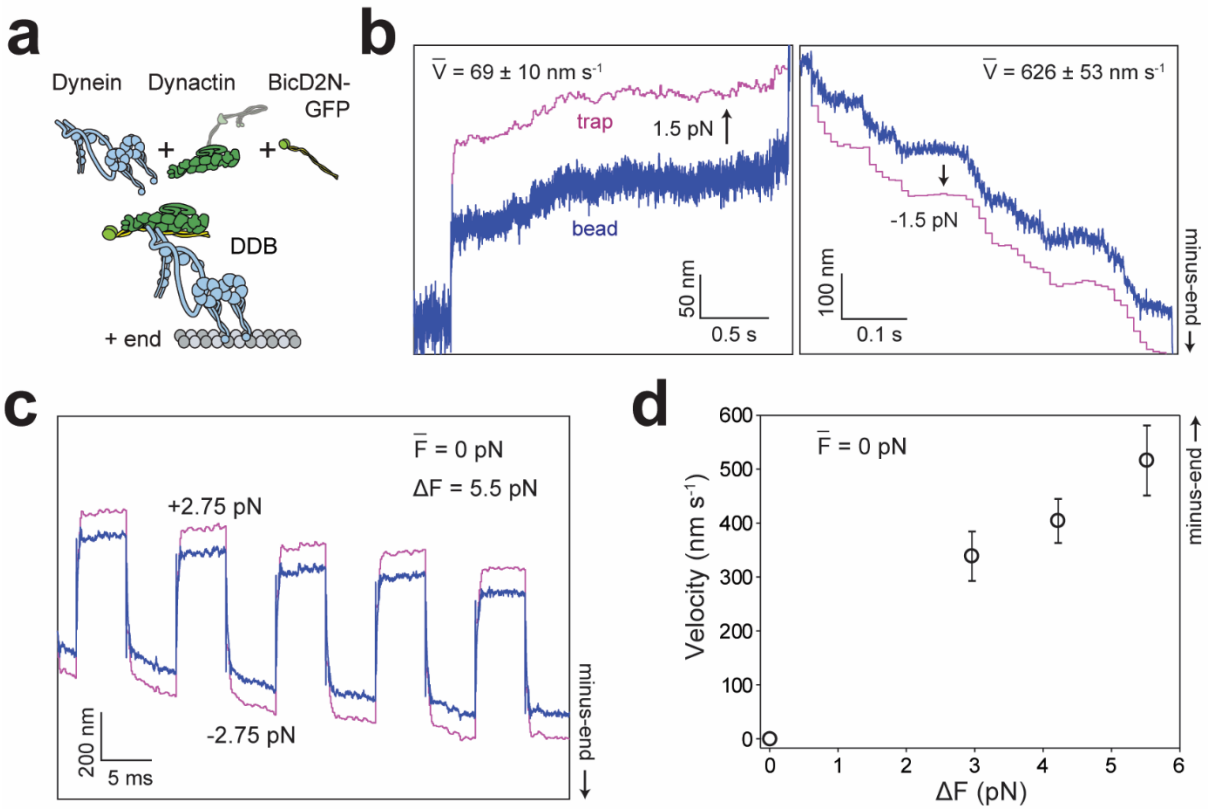

Figure 13. Force oscillations facilitate ratcheting of mammalian dynein-dynactin towards the minus-end of MTs in the absence of ATP. a. *The assembly of the DDB complex from human dynein, pig-brain dynactin and the N-terminal coiled-coil of mouse BicD2 (BicD2N, 1-400). BicD2N was fused with GFP at its C-terminus for attachment of the complex to antiGFP-coated beads.* ***b.*** *Example trajectories of DDB-driven beads pulled towards the MT plus- (left) and minus- (right) end under 1.5 pN force. The average velocities (mean ± s.e.m.) were calculated from 44 (left) and 27 (right) trajectories.* ***c.*** *Example trajectory of a human dynein-driven bead oscillated ±2.75 pN in a square wave pattern at 10 Hz shows processive motility towards the MT minus-end.* ***d.*** *The velocity of dynein-driven beads increases with ΔF in the absence of net force on the bead (mean ± s.e.m.; from left to the right n = 25, 32, 26 from three technical replicates). In comparison, DDB ratcheted faster towards the MT-minus-end than S. cerevisiae dynein.*

Force oscillations increase cargo transport and MT gliding velocity

We next tested our prediction that dynein's ratcheting along MT increases the velocity and stall force under physiological ATP concentrations (Figure 14a). We measured the velocity of dynein-driven beads subjected to force oscillations in 1 mM ATP (Figure 14b). At $\bar{F} = 0\ pN$, application of ΔF up to 4.2 pN increased the velocity by 67% (190 ± 11 nm s^{-1}, Figure 14c), demonstrating that dynein moves faster by harnessing the energy of force fluctuations under saturating ATP.

ATP is abundant inside the cell and dynein can benefit from the force fluctuations that already exist in the cell to become a better minus-ended motor and withstand higher forces. Dynein motors in cells also anchor onto large organelles or the plasma membrane and pull the MTs. Therefore, it's also important to understand the collective behavior of dyneins under physiologically relevant conditions.

To test whether oscillations of the MT network affect the MT sliding activity by multiple dyneins, we oscillated beads attached to MTs as they are glided by surface-immobilized dyneins (Figure 14d). In order to initiate force oscillations before the beads escape the trap, we lowered gliding velocity under no force to 23 ± 2 nm s^{-1} (mean ± s.e.m.) by reducing ATP concentration to 20 µM. Trajectories revealed that assisting forces significantly increased the gliding velocity whereas hindering forces caused a modest slowdown of MT gliding (Figure 14e). In the absence of net force, the application of ΔF up to 6.3 pN caused a two-fold increase in gliding speed (Figure 14f), demonstrating that the periodic oscillation of MTs leads to faster filament sliding activity of dynein motors.

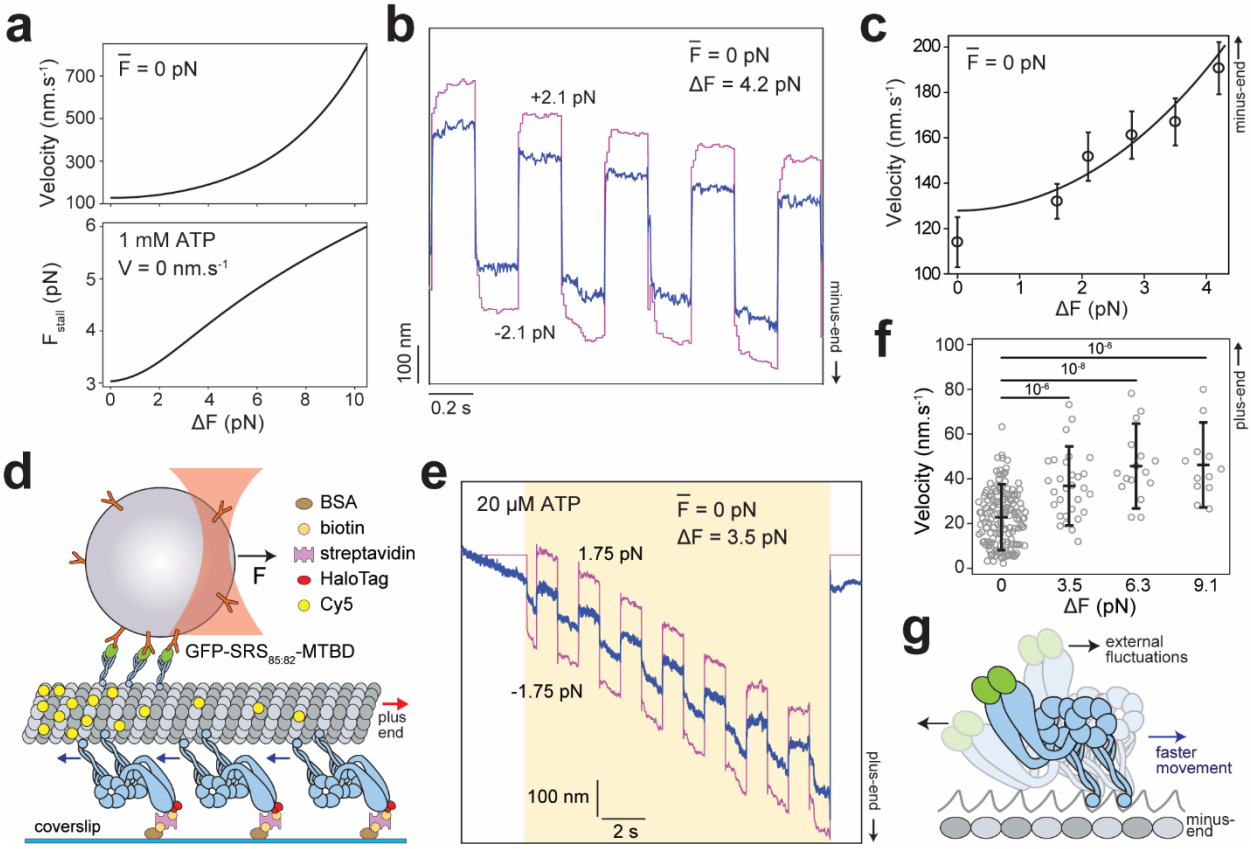

Figure 14. Force oscillations increase cargo transport and MT gliding velocity of dynein in the presence of ATP. a. *The estimated velocity and stall force of dynein under force oscillations are calculated from the F-V curve in Figure 8c.* ***b.*** *Example trajectory of a dynein-driven bead oscillated ±2.1 pN at 2.5 Hz.* ***c.*** *The velocity of dynein-driven beads increases by the increase in ΔF on the bead (mean ±*

s.d.; n = 78, 42, 35, 28, 30, 21 from left to right from three technical replicates). The black curve shows the estimated velocities in (a). ***d.*** *Schematic of the optical trapping assay for the MT oscillations. Dyneins were fixed on the glass surface from their tail through a biotin-streptavidin linkage. MTs glide with their plus-end in the lead (red arrow) due to the minus-end-directed motility of surface-immobilized dyneins (blue arrow). The trapped bead was tightly attached to a gliding MT on the surface and oscillated back and forth at 1 Hz.* ***e.*** *Example trajectory of a gliding MT oscillated ±1.75 pN at 1 Hz in 20 μM ATP. The yellow shaded region represents duration the force-feedback is engaged for trap oscillations.* ***f.*** *MT gliding velocity increases by the magnitude of force fluctuations. Data at 0 pN were obtained from fluorescence experiments. The center line and edges represent mean and s.d., respectively. p values are calculated from Welch's t-test (n = 144, 30, 16, 12 from left to right).* ***g.*** *Due to the asymmetric force-detachment kinetics, dynein ratchets towards the minus-end of MTs under external fluctuations.*

Discussion

Collectively, our results show that dynein forms an asymmetric slip bond with a MT, which enables this motor to harness energy from cytoskeletal fluctuations (Figure 14g). Unlike myosin V that functions as a reverse ratchet [111], dynein is a forward ratchet that favors faster movement when pulled towards its natural direction of motion. Therefore, fluctuations increase the speed of dynein motility and the ability of the motor to resist hindering forces, resulting in higher power output (Figure 15).

The ratcheting mechanism is especially useful for dynein in the presence of ATP. The estimated power output differs drastically for no-ATP (Figure 15c) and ATP conditions (Figure 15d) for the same ΔF.

It is possible that ratcheting along MTs may assist dynein to perform its cellular functions. Dynein carries organelles and vesicles towards the nucleus of interphase cells and drives retrograde transport towards the cell body in neurons[10]. Dyneins also generate periodic oscillations of MTs from millisecond to minute timescales[112]. During asymmetric cell division, the entire mitotic spindle undergoes periodic oscillations due to antagonistic force generation of cortical dyneins and this is attributed to force-dependent detachment of dynein from an MT[113, 114]. Ratcheting may enable dyneins to move towards the minus-end at faster speeds and increase tension for proper positioning of the spindle[23]. Similarly, the beating of motile cilia is powered by antagonistic forces generated by axonemal dyneins on either side of an axoneme. Active oscillations of the parallel bundle of MTs may increase the MT sliding velocity of axonemal dyneins (Figure 14) and the frequency of ciliary beating[115, 116]. Our oscillating trap assay can be combined with efforts on *in vitro* reconstitution of the mitotic spindle[117] and cilia-like beating of MT bundles[118] for testing these ideas.

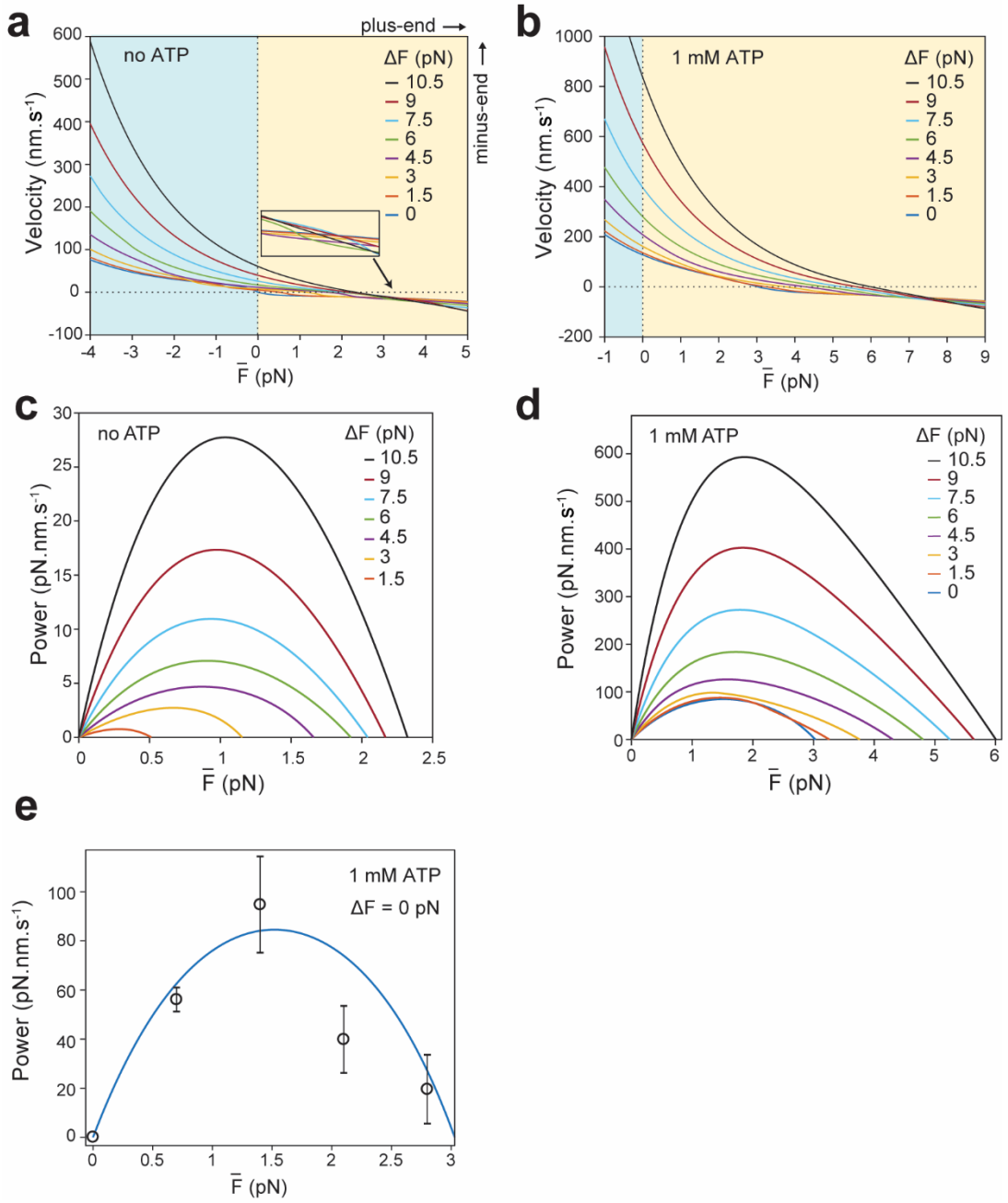

Figure 15. Force fluctuations increase the power output of dynein towards the minus-end. a-b. *Estimated* $\bar{F} - V$ *relationship under different ΔF in the absence (a) and presence (b) of 1 mM ATP. The model predicts that increasing ΔF leads to faster minus-end directed velocities at* $\bar{F} = 0$ *pN and higher average hindering forces to stall the bead movement. The inset in (a) shows that the curves do not intersect at the same point.* ***c-d.*** *Force oscillations increase the power output of dynein in the absence (c) and presence (d) of 1 mM ATP. The power output of dynein at average hindering forces was calculated from the F-V relationship.* ***e.*** *Power output of dynein (black circles, mean ± s.e.m.; n = 42, 56, 58, 47 from left to right) in 1 mM ATP and in the absence of force fluctuations (ΔF = 0 pN). The blue curve corresponds to the 0 pN curve in d.*

Methods

Protein purification and labeling

Full-length *S. cerevisiae* dynein was tagged with GFP at its N-terminus and a HaloTag (DHA) at its C-terminus, and expressed under the native promoter[65]. To construct monomeric dynein, the 5' end of the dynein gene encoding the tail was deleted leaving amino acids 1219-4093 with predicted molecular weight of 331 kDa. The construct was tagged with GFP at its N-terminus and DHA at its C-terminus and expressed under a galactose promoter (GFP-Dyn_{331kD}-DHA)[65]. For MT gliding assays, a GST dimer of tail truncated dynein was tagged with DHA at the N -terminus (DHA-GST-Dyn_{331kD})[65]. These constructs were purified from *S. cerevisiae* cultures by incubating the cell lysate with IgG beads (GE Healthcare) and eluting the protein from beads using Zz-Tev cleavage, as described previously[65]. The motor was labeled with 10 μM tetramethylrhodamine (TMR)- or biotin-alkyl chloride (a HaloTag ligand) at the DHA tag for additional 1 h at 4 ℃ before cleaving the protein from IgG beads. For DNA-tethered optical trapping experiments, a 74 bp double-stranded DNA tether was labeled with biotin in one end and alkyl chloride-NHS at the opposite end, and excess ligand was removed using ethanol precipitation at 4 ℃, as previously described[83]. 10 μM DNA tether was incubated with monomeric dynein for additional 1 h at 4 ℃ before cleaving the protein from IgG beads.

The constructs that express a phi mutant of human dynein (SNAP-$DYNC1H1_{E1518K/R1567K}$) in a pACEBac1 vector backbone[119]; the pDyn2 plasmid that contains genes from IC2C, LIC2, TCTEX1, LC8, and ROBL1, and mouse BICD2-400-GFP (BicD2N-GFP) in a pOmniBac vector backbone were provided by A. P. Carter[69]. Human dynein and BICD2N constructs contain 6x-His-ZZ tag followed by a TEV protease cleavage site for protein purification. The proteins were expressed using the baculovirus insect cell system, and purified using Tev cleavage from IgG beads, as described previously[120]. Dynactin was purified from pig brain using the large-scale SP-Sepharose and MonoQ ion exchange chromatography[64]. The 6x-His-tagged GFP-$SRS_{85:82}$-MTBD construct was expressed in *E. Coli* and purified using NiNTA affinity purification, as previously described[121]. Purified protein was aliquoted and flash frozen in liquid nitrogen. Protein purity was confirmed with gel electrophoresis and the concentration was measured using the Quick Start Bradford kit (BioRad).

Coating beads with anti-GFP antibodies

Carboxyl latex beads (860 nm in diameter, Life Technologies) were coated with custom-made rabbit polyclonal anti-GFP antibodies (Covance). 200 μL of beads were resuspended three times in activation buffer (10 mM MES pH 6.0, 100 mM NaCl) after spinning down at 8,000 rpm for 3 min. 1 mg of EDC and 1 mg of S-NHS were dissolved in 1 mL and 2 mL DMF, respectively and 20 μL of dissolved EDC and 40 μL of dissolved S-NHS were added to beads. The beads were sonicated for 3 min and nutated at low speed until visible clumps disappeared. The beads were

rinsed in PBS (phosphate buffered saline, pH 7.4) buffer in 800 µL total volume and reacted with 200 µL of 0.4 mg ml^{-1} of antibody. After shaking the mixture for 30 min, the beads were passivated by adding 10 mg ml^{-1} BSA for 2 h, washed in PBS three times and stored in PBS supplemented with 0.1% sodium azide and 0.5 mg ml^{-1} BSA at 4 °C.

Sample Preparation

Cy5-labeled axonemes were flown into the chamber in DLB buffer (30 mM HEPES pH 7.2, 2 mM $MgCl_2$, 1 mM EDTA, 10% glycerol). To determine the polarity of axonemes, a TMR-labelled DHA-GST-Dyn_{331kD} was flown into the chamber with 1 mM ATP in DLBC buffer (DLB supplemented with 1 mg ml^{-1} casein and 2 mM DTT). After waiting for 5 min to allow dynein to accumulate at the MT minus-end, the chamber was washed three times with 30 µl DLBC. GFP-tagged *S. cerevisiae* dynein was mixed with antiGFP-coated beads for 10 mins on ice. For DNA-tethered optical trapping experiments, monomeric *S. cerevisiae* dynein labeled with a DNA tether was incubated with streptavidin-coated polystyrene beads (860 nm in diameter, Spherotech) for 5 mins on ice. The motor-bead mixture was introduced into the chamber along with 1 mM ATP and the oxygen scavenger mixture (35 mg ml^{-1} protocatechuic acid (PCD) and 2.5 mM protocatechuate-3,4- dioxygenase (PCA)).

For trapping experiments with mammalian dynein-dynactin, DDB complexes were assembled by mixing 1 µl of 1.2 mg ml^{-1} dynein with 1 µl of 1.6 mg ml^{-1} dynactin, and 1.5 µl of 3-4 mg ml^{-1} cargo adaptor (BicD2N-GFP) in 10 µl dynein motility buffer (DMB: 30 mM HEPES pH 7.0, 5 mM $MgSO_4$, 1 mM EGTA, 1 mM TCEP (tris(2- carboxyethyl)phosphine) supplemented with 1 mg ml^{-1} bovine serum albumin (BSA). The complex was incubated on ice for 10 min. The complex assembly was incubated with antiGFP- coated beads for 10 mins on ice, diluted in DMB supplemented with 1.25 mg ml^{-1} casein (DMB-C), 5 U ml^{-1} of apyrase, 2.5 mM PCA (protocatechuic acid) and 50 nM PCD (protocatechuate-3,4-dioxygenase), and flown into the chamber.

To ensure that more than 95% of the beads are driven by single dyneins, the motor to bead ratio was reduced until less than 30% of the beads walk along MTs in the presence of ATP. To test the motility of dynein-driven beads in the absence of nucleotide, instead of 1 mM ATP, 5 U ml^{-1} of apyrase was added to the motor-bead mixture to deplete the residual ATP in the chamber.

Microtubule gliding assays

To polymerize MTs, unlabeled and Cy5-labeled pig tubulin were mixed in BRB80 buffer (80 mM PIPES pH 6.8, 1 mM $MgCl_2$, 1mM EGTA, 1mM DTT) supplemented with the polymerization mixture (2 mM GTP, 20% Dimethyl sulfoxide (DMSO) in 2x BRB80). MTs were polymerized for 20 min at 37 °C. 10 µM taxol was added to the mixture and incubated for an additional 10 min at 37 °C. Excess tubulin was removed by pelleting and resuspending MTs

at 20,000 g for 12 min in BRB80 supplemented with 10 μM taxol. MTs were stored at room temperature in dark.

To exert forces on MTs during gliding motility, beads were densely coated with a construct that contains dynein MTBD and part of the stalk coiled-coil fused to monomeric seryl-tRNA synthetase (GFP-$SRS_{85:82}$-MTBD)[30]. 2 μl of 5 μM GFP-$SRS_{85:82}$-MTBD was incubated with 1 μl of 4% v/w bead solution for 5 min. Excess protein was removed by addition of 1 ml DLB, and pelleting and resuspending the beads in 5 μl DLB. DHA-GST-Dyn_{331kD} was labeled with biotin at the N-terminus and fixed onto the glass surface through a BSA-biotin and streptavidin linkage. The sample was washed with DLB, and 10 μl of 0.1 mg ml^{-1} Cy5 MTs were introduced to the chamber in the presence of 10 μM taxol. After 2 min incubation, 40 μl of 20 mg ml^{-1} beads were introduced to the chamber in DLB supplemented with 20 μM ATP, 10 μM taxol, oxygen scavenger mixture (2.5 mM PCA and 50 nM PCD) and the ATP regeneration mixture (2 mM phosphoenolpyruvate and 0.42 mM pyruvate kinase).

Optical Trapping Assays

All trapping experiments were performed on a fully automated optical trap that was custom-built in an acoustically isolated and temperature-controlled (±0.1 °C) room around the body of a Nikon Ti-E inverted microscope[83]. Beads were trapped using a 2 W 1064 nm laser (Coherent). The trapping beam was focused on the image plane using a 100 x 1.49 N.A. apochromat oil-immersion objective (Nikon). Cy5-labeled axonemes or MTs were excited using a 632 nm HeNe laser (Melles Griot) and imaged via a monochrome CCD camera (The Imaging Source). MTs were moved to the center of the field of view using a locking XY stage (M-687, Physik Instrumente). A pair of perpendicular acousto-optical deflectors (AODs, AA Optoelectronic) were placed in a plane conjugate to the back focal plane of the objective to steer the trap. The laser power was adjusted with a half-wave plate on a motorized rotary mount (New Focus). Beads were lowered on the axonemes using a piezo flexure objective scanner (P-721 PIFOC, Physik Instrumente). Bead position relative to the center of the trap was determined by imaging the back-focal plane of a 1.4 N.A. oil immersion condenser (Nikon) on a position-sensitive detector (First Sensor). Calibration of the detector response was performed by raster-scanning the laser across a trapped bead with the AOD[12]. The power spectrum of a trapped bead position was fit to a Lorentzian to obtain the trap stiffness.

Freely diffusing monodisperse beads were trapped and lowered onto a surface-immobilized Cy5-labeled axoneme oriented parallel to the PSD horizontal axis. To perform constant force assays in the presence of ATP, force-feedback control was activated after the beads moved 40 nm away from the trap center. In the absence of ATP, MT polarity was determined by allowing TMR-labeled dynein to walk on axonemes for 5 min and accumulate at the minus-end before washing the assay solution and replacing it with the bead-motor mixture and apyrase. A trapped bead was lowered onto an axoneme and briefly released and trapped until it binds to an MT. Force feedback was applied in forward or backward directions. The magnitude of the applied force was adjusted by changing the laser power while keeping the bead-trap separation at 100 nm. The

bead position was acquired at 5 kHz and the trap position was updated at 100 Hz to keep the bead-trap separation constant. The trap stiffness was set to 37.5 fN nm^{-1}. The thermal relaxation of the bead (300 Hz) was taken to be roughly equal to the corner frequency of the trap.

Force oscillation experiments were performed using the force-feedback controlled trap. The applied force was alternated periodically in a square wave pattern at 2.5 Hz. To enable for more rapid and accurate switching between the assisting and hindering forces, we commanded the trap to move by an experimentally estimated offset every time it switched between the forward and backward feedback setpoints. This compensated for the free rotation of the bead, which results in a movement without a net force exerted on the bead. This "dead" region corresponds to the 250-500 nm difference between bead positions under the forward and backward pull of the trap, despite the motor remains attached to the MT. For experiments with zero $\bar{F}$ on the bead, the bead-trap separation was kept constant at 100 nm and the trap stiffness was adjusted to apply desired forces on the bead. In experiments where ΔF was kept constant, force bias was provided by using different trap-bead separation distances when the bead was pulled towards the plus- and minus-ends of an MT. Over 90% of the applied force was along the long axis of the MT, whereas the short axis deviated from the trap center negligibly during data collection.

For the release rate measurements, beads were sparsely coated with tail-truncated dynein monomers (GFP-Dyn_{331kD}-DHA)[65] were brought onto an axoneme and oscillated with a period of 0.7 s between two positions (±100 nm). MT polarity was determined using TMR-labeled dynein, as described above. The bead position was fitted to a step-finding algorithm[12] to detect individual release events. The bead to motor ratio was adjusted such that more than 80% of release events occurred in a single step. Release events occurred in more than a single step and dwells shorter than 3 ms were discarded from the analysis. Release data were sorted and binned by force. Cumulative distribution of each bin was fitted to a double exponential decay to determine fast (k_1) and slow (k_2) release rates. This is in comparison to using the histograms of the MT residence times for fitting, which would yield release rates that depend on the histogram bin size[77]. The double exponential decay fit was statistically justified using the F-test. In MT gliding assays, the surface density of dynein was sufficient to glide MTs on a straight path for several microns over the course of force application. Freely diffusing polystyrene beads were lowered to a gliding MT between 4 to 10 μm in length. These beads were tightly bound to the MT as soon as they were in contact with each other. After MT binding, the force-feedback controlled trap was engaged and the bead was pulled along the MT long axis back and forth at 2.5 Hz. The beads remained firmly attached to MTs during force oscillations. External force did not alter the direction of gliding motility. The bead-trap separation was kept at 100 nm and forces on the bead were adjusted by altering the trap stiffness.

Data Analysis

Traces were recorded at 5 kHz, down sampled to 500 Hz and visualized using custom software written in MATLAB. Trajectories that contain instantaneous jumps greater than 40 nm were either excluded from the data analysis because this distance exceeds the maximum size of the

steps that dynein takes. For the force velocity measurements, the minimum accepted run time was 200 ms. The velocity was calculated by dividing the total distance traveled to the elapsed time during force application. Power was calculated by the multiplication of the average force on the bead and velocity of the motor movement. For step size analysis, trajectories were downsampled to 100 Hz, and fit to a step finding algorithm using the Schwartz Information Criterion[83]. Step size versus force graphs in Supplementary Figs. 3c and 4c were interpolated using an exponential function. The step size was set to zero at 0 pN in no ATP, and at 3.1 pN in 1 mM ATP condition.

3. Future Directions

Understanding the release rate of a dynein monomer was critical to model how constant and fluctuating forces affect the velocity of a dynein dimer. These experiments assume that the trap only pulls the bead in the forward or backward directions. However, recent studies have investigated a possible drawback of the single bead attachment geometry in optical trap[105, 122]. Khataee et al[105] has suggested that, in the single bead geometry (which is drawn closer to the scale in Figure 16), motors feel force not only along the MT long axis but also towards the z-direction (Figure 16). This is especially critical for kinesin motors where studies have shown that kinesin prematurely releases from the MT before the motor comes to a complete stall. In comparison, a dynein dimer stalls on an MT for several seconds before dissociation. In addition, the stall force of a bead does not increase substantially when multiple kinesins are tied together, suggesting that individual kinesins release from MT before they come to a complete stall[123]. In contrast, the stall force increases linearly with increasing dynein copy number[61]. The difference between dynein and kinesin may arise from their unique structural organization and the way they interact with the MT. As a result, the z-force may be affecting kinesin force measurements more than dynein.

A recent study by Brenner et al. has investigated the possibility of limitation of force-production of several motors due to their low processivity[124]. They have found that mammalian dynein by itself fails to produce a maximal amount of force under low trap stiffness because of its short run length. In other words, because the motor is not very processive without its cofactors, it unbinds from the MT before it can produce a larger force. However, increasing the trap stiffness did not have any effect on yeast dynein, and kinesin produced less force only at higher salt conditions. Therefore, the presence of z-force remains to be a better explanation for the premature release of kinesins and partially-active mammalian dynein motors from MTs.

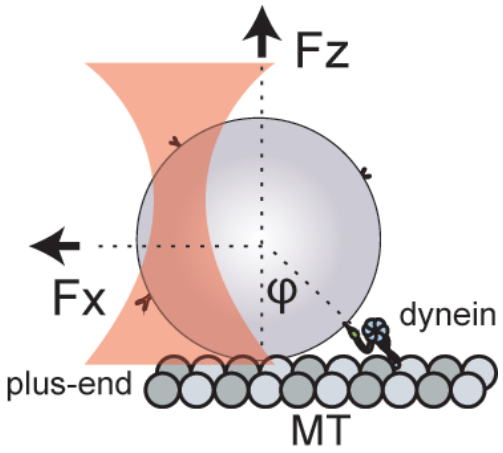

Figure 16. Motor proteins are a lot smaller than the bead in an optical trap. *Motor proteins may be exerted a force in the z-direction which would increase the release rate in both forward and backward directions. Typical bead size is 860 nm in diameter whereas dynein is only 40 nm in length.*

The fact that multiple kinesins do not generate more force has been attributed to the geometrical design used in the optical trap experiments. Models on cargo transport by multiple kinesins have assumed that kinesin has a symmetric force-detachment profile; however, recent studies by S. Block and coworkers[125] have shown that a single kinesin releases more easily under assisting loads compared to the hindering loads. The model by Khataee et al. suggests that the net force acting on a bead has both vertical (F_z) and horizontal (F_x) components, and argues that the vertical force component is dominant in the release rate, hence giving rise to a more symmetric force-detachment profile. Furthermore, in a simple approach where the bead contacts the MT, the value of F_z is determined by the formula:

$$F_x/F_z = \tan\varphi$$

where φ is the angle between the motor and the z-axis (Figure 16).

This theory has been further supported by Pyrpassopoulos et al.[122] where they used a three-bead assay to study the stalling behavior of single and multiple kinesins. Here, the contact of a single bead with the MT accelerated the detachment of the kinesins from the MT. Remarkably, the three-bead assay resulted in a median value of attachment durations that were 10-fold longer compared to the single bead assay. In other words, kinesin consistently stalled for longer times in the three-bead assay geometry compared to rare stalling events in the single bead assay. Moreover, multiple kinesins showed higher stall forces, which has not been the case with the single bead geometry.

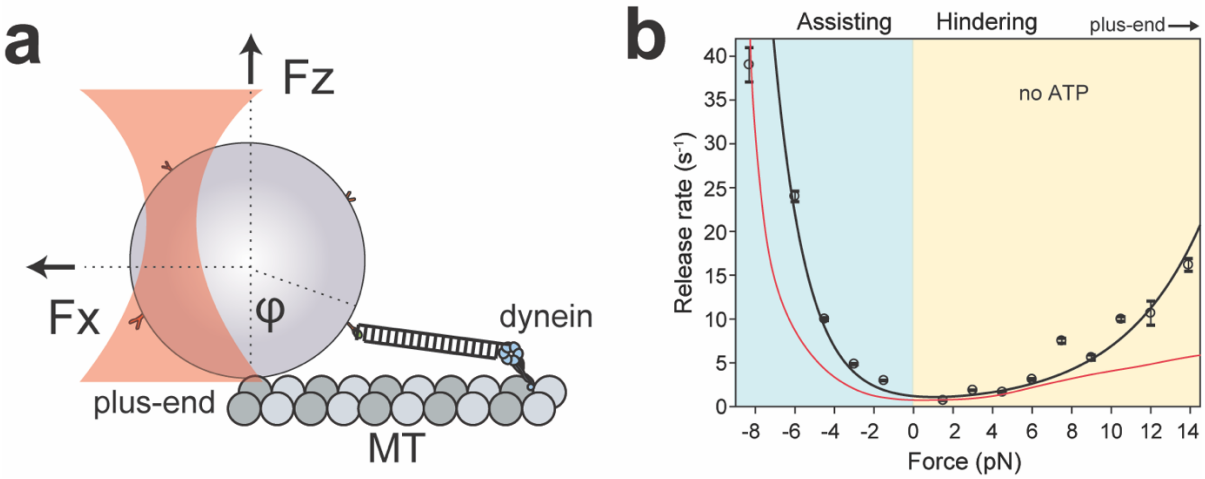

Figure 17. Dynein may have a more asymmetric release rate profile. a. *The proposed experiment with a long DNA tether would alter the angle φ and decrease F_z.* ***b.*** *Dynein monomers may have a more asymmetric release rate profile as shown in the hypothetical profile (red) compared to the experimental values obtained in a single bead optical trapping technique (Figure 6c)*

These studies strongly suggest that motor force measurements need to be repeated in the absence of vertical forces, which may be an artifact of the single bead assay geometry. The z-force can be reduced drastically by using long DNA tethers to connect the motor and the bead as seen in

Figure 17. The bead size is another parameter that would affect the angle and smaller beads can be used to decrease the angle φ and further reduce the z-force.

Let's imagine the following scenario to understand how a longer tether and a smaller bead would affect the magnitude of F_z. My previous oscillation experiments on dynein have revealed that a bead center swings around 200 nm in both directions (Figure 11d). This value is approximate and depends on where the connection between the bead and the motor happens. Assuming a bead with a diameter of 860 nm is used; the angle φ is calculated by $\sin\varphi = swing\ distance/radius$ which is around 27°. According to this, F_z is expected to be ~5.5 pN when F_x is 3 pN. A 3 kbp DNA tether reduces F_z to ~1 pN. And a smaller bead with a 500 nm diameter scales F_z down to ~0.6 pN when F_x is 3 pN. Therefore, it is theoretically possible to decrease the vertical force to its one-tenth using this approach.

Such an experiment can be designed as follows. A long 3 kbp double stranded DNA is obtained from lambda phage DNA through PCR using two primers. One of the primers terminating with biotin is linked to the streptavidin beads. The second primer terminating with amino group is labeled with alkyl chloride NHS and linked to the motor tagged with a HaloTag.

If z-force affects dynein as substantially as it affects kinesin, it would prove dynein to be an even stronger ratchet than we measured here and dynein can harness even more energy from the active fluctuations inside the cell. The new release rate profile would look more like the red curve in Figure 17b where release rates in both directions decrease but the overall asymmetry increases. This may also increase the observed asymmetry in the force-velocity curves obtained in Figure 8.

These future experiments may have strong implications for the way motors drive bidirectional transport along MTs. Live cell imaging studies revealed that most cargos simultaneously recruit kinesin and dynein motors[126-128]. It remains unclear how the activities of these opposite polarity motors are regulated to drive transport. In certain cases, it is well established that the motor activity is tightly regulated, such that only one motor type remains active at a time, while the other motor is transported as an inactive cargo. Therefore, the cargo moves at the full speed of the winning motor and can start moving backward as soon as the motors are switched at turnaround zones. In other cases, the cargo movement is saltatory, in which unidirectional movement is interspersed with frequent and brief pauses[129]. The prevailing model, in this case, is a motor tug-of-war: both motor types are actively pulling in the opposite direction and the cargo moves in the direction of the net force vector[130].

In the case of tug-of-war, the losing motors are expected to step processively backward under the pulling forces of the winning motor[130]. Single bead optical trapping experiments showed that such mechanism is feasible, as both kinesin and dynein have been shown to walk backward under superstall forces. However, this backward movement is usually much slower than the full motor speed in the forward direction, whereas the speed of intracellular cargos is usually at the rate of full motor speed as the cargo moves unidirectionally in between pauses. Therefore, it is not clear where the tug-of-war model can account for the saltatory movement of intracellular cargos.

DNA-tethered bead trapping measurements may reveal that both kinesin and dynein motors respond more asymmetrically to external forces than previously thought by classical single bead experiments. If kinesin releases when pulled towards the plus end, but not the minus end, and vice versa for dynein, this would strongly indicate that either motor is unlikely to step backward when competing against the opposite polarity motor. Therefore, these studies can potentially show that intracellular transport cannot be driven by the motor tug of war. Instead, the motors may be switched on and off in trans, as in the case of tightly controlled transport, but this regulatory mechanism may be more transient, leading to frequent pauses and backward movements in cargo movement before it reaches to its destination.

3. Theory

The force-detachment kinetics of a dynein monomer

Case 1: no ATP, no force

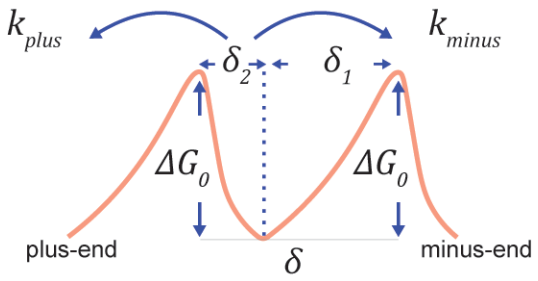

The free energy landscape of dynein-MT interaction has a barrier width of δ. The distance to release towards the minus-end is $\delta_1 = \frac{\delta}{2} + A$ and the distance to release towards the plus-end is $\delta_2 = \frac{\delta}{2} - A$, where A is the asymmetric distance parameter. In the absence of ATP, the barrier height is ΔG_0. In the absence of ATP and force, forward (k_{minus}) and backward (k_{plus}) release rates are equal to k_0^{apo}:

$$(1) \qquad k_{minus} = k_{plus} = k_0^{apo} = Be^{-\Delta G_0/k_B T}$$

where B is the Arrhenius frequency factor, k_B is the Boltzmann constant and T is the absolute temperature.

Case 2: no ATP, hindering force

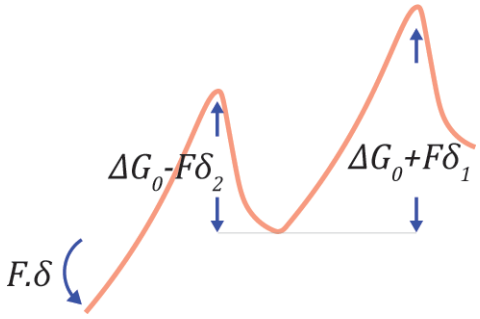

The work done by the hindering force ($F\delta > 0$) shears the energy landscape towards the plus-end, lowering the barrier height for release towards the plus-end, while increasing the barrier for

release towards the minus-end direction. Because of the asymmetry, the shearing of the barrier height is not equal in plus and minus directions.

$$(2) \qquad k_{minus} = k_0^{apo} e^{-F(\frac{\delta}{2}+A)/k_BT},\ k_{plus} = k_0^{apo} e^{F(\frac{\delta}{2}-A)/k_BT}$$

As a result, under the same magnitude of force, k_{plus} increases more slowly under hindering forces *(F)* compared to k_{minus} under assisting forces *(-F)*.

Case 3: 1 mM ATP, no force

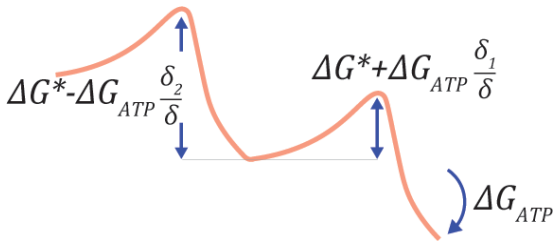

In the presence of saturating ATP, the energy barrier to release (ΔG^*) is lower than the apo condition. In addition, the free energy of ATP hydrolysis ($\Delta G_{ATP} < 0$) shears the energy landscape towards the minus-end. In this case,

$$(3) \qquad k_0^{ATP} = Be^{-\Delta G^*/k_BT}$$

$$(4) \qquad k_{minus} = k_0^{ATP} e^{-\Delta G_{ATP}\frac{1}{\delta}(\frac{\delta}{2}+A)/k_BT},\ k_{plus} = k_0^{ATP} e^{\Delta G_{ATP}\frac{1}{\delta}(\frac{\delta}{2}-A)/k_BT}$$

Case 4: 1 mM ATP, hindering force

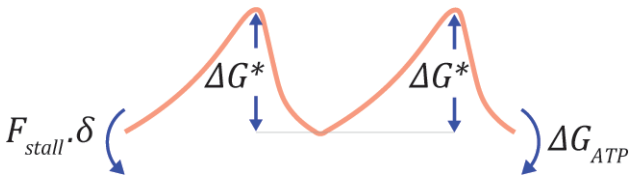

Hindering force and ATP hydrolysis perform works against each other. In this case,

$$(5) \qquad k_{minus} = k_0^{ATP} e^{-(F+\frac{\Delta G_{ATP}}{\delta})(\frac{\delta}{2}+A)/k_BT},\ k_{plus} = k_0^{ATP} e^{(F+\frac{\Delta G_{ATP}}{\delta})(\frac{\delta}{2}-A)/k_BT}$$

When the work done by external force ($F\delta$) is equivalent to $-\Delta G_{ATP}$,

(6) $k_{minus} = k_{plus} = k_0^{ATP}$

and the motor comes to a stall ($V = 0$, see below). Therefore,

(7) $F = F_{stall} = -\Delta G_{ATP} \,/\, \delta$

The force-velocity relationship of a dynein dimer

Case 1a: Constant step size, no ATP

In this case, we assume that dynein has a constant step size of *d* in the minus-end and *-d* in the plus-end direction and the step sizes do not change by external force. Using equation 2, the F-V relationship can be explained as follows:

(1) $V = \ (k_{minus} - k_{plus})d = \ 2dk_0^{apo} e^{-\frac{F\,A}{k_B T}} sinh\left(\frac{-F\delta}{2k_B T}\right)$

In the presence of oscillatory forces, we define

(2) $\bar{F} = \frac{F_{plus} + F_{minus}}{2}$

(3) $\Delta F = \ F_{plus} - F_{minus}$

The ΔF-V relationship in the absence of net force is

(4) $V(\Delta F)_{\bar{F}=0} = \frac{V(\frac{\Delta F}{2}) + V(-\frac{\Delta F}{2})}{2}$

(5) $V(\Delta F)_{\bar{F}=0} = 2dk_0^{apo} sinh\left(\frac{\Delta FA}{2k_B T}\right) sinh\left(\frac{\Delta F\delta}{4k_B T}\right), \ \ \Delta F > 0$

The $\bar{F}$-V relationship in the presence of constant ΔF is

(6) $V(\bar{F})_{\Delta F} = \frac{V(\bar{F} + \frac{\Delta F}{2}) + V(\bar{F} - \frac{\Delta F}{2})}{2}$

Case 1b: Constant step size, saturating ATP

In the presence of saturating ATP, the F-V relationship can be determined using equations 4 and 7 as follows:

$$(7) \qquad V = (k_{minus} - k_{plus})d = 2dk_0^{ATP} e^{-\frac{(F-F_{stall})A}{k_BT}} sinh\left(\frac{-(F-F_{stall})\delta}{2k_BT}\right)$$

The ΔF-V relationship in the absence of net force is calculated using equation 12.

The $\bar{F}$-V relationship in the presence of constant ΔF is calculated using equation 13.

Case 2a. Variable step size, no ATP

Because the average forward and backward step sizes of dynein are markedly different and they are force-dependent (Figure 9c), we take this variability into account as follows:

$$(8) \qquad V(F) = k_{total}(F)d(F) \qquad where\ k_{total} = k_{minus} + k_{plus}$$

We note that *d(F)* is defined as the average of all steps taken by dynein at a given load. The steps in the minus-end direction have positive values, whereas steps in the plus-end direction are negative. *V(F)* and *d(F)* are measured by experiments (Figure 8b and Figure 9c). The ratio of these measured values was fit to a model as follows:

$$(9) \qquad \frac{V(F)}{d(F)} = k_{total}(F) = 2k_0^{apo} e^{-\frac{FA}{k_BT}} cosh\left(\frac{F\delta}{2k_BT}\right)$$

to estimate k_0^{apo}, A and δ (see Figure 9d).

In order to show the fit on the F-V curve (Figure 8b), *V(F)* is calculated by

$$(10) \qquad V(F) = k_{total}(F)d_{interpolated}(F)$$

where $k_{total}(F)$ is the fit shown in Figure 9d and $d_{interpolated}(F)$ is the fit shown in Figure 9c.

Case 2b. Variable step size, saturating ATP

In the presence of saturating ATP, the ratio of measured velocities (Figure 8c) to step size (Figure 10c) was fit to

$$(11) \qquad \frac{V(F)}{d(F)} = 2k_0^{ATP} e^{-\frac{(F-F_{stall})A}{k_BT}} cosh\left(\frac{(F-F_{stall})\delta}{2k_BT}\right)$$

to estimate k_0^{ATP}, F_{stall}, A and δ (see Figure 10d).

In order to show the fit on the F-V curve (Figure 8c), *V(F)* is calculated by equation 17 where $k_{total}(F)$ is the fit shown in Figure 10d and $d_{interpolated}(F)$ is the fit shown in Figure 10c.

In cases 2a and 2b, the ΔF-V relationship in the absence of net force (Figures 11d and 14c) and the $\bar{F}$-V relationship in the presence of constant ΔF (Figure 11f) are calculated using equations 12 and 13.

5. References

1. Schliwa, M. Myosin steps backwards. *Nature* **401**, 431-432 (1999).
2. Wells, A.L. *et al.* Myosin VI is an actin-based motor that moves backwards. *Nature* **401**, 505-508 (1999).
3. Paschal, B.M. *et al.* Isolated flagellar outer arm dynein translocates brain microtubules in vitro. *Nature* **330**, 672-674 (1987).
4. Vale, R.D., Reese, T.S. & Sheetz, M.P. Identification of a novel force-generating protein, kinesin, involved in microtubule-based motility. *Cell* **42**, 39-50 (1985).
5. Cho, C., Reck-Peterson, S.L. & Vale, R.D. Regulatory ATPase sites of cytoplasmic dynein affect processivity and force generation. *The Journal of biological chemistry* **283**, 25839-25845 (2008).
6. Verkhovsky, A., Svitkina, T. & Borisy, G. Myosin II filament assemblies in the active lamella of fibroblasts: their morphogenesis and role in the formation of actin filament bundles. *J Cell Biol* **131**, 989-1002 (1995).
7. Yildiz, A. *et al.* Myosin V walks hand-over-hand: single fluorophore imaging with 1.5-nm localization. *Science* **300**, 2061-2065 (2003).
8. Hirokawa, N., Noda, Y., Tanaka, Y. & Niwa, S. Kinesin superfamily motor proteins and intracellular transport. *Nature reviews. Molecular cell biology* **10**, 682-696 (2009).
9. Yamada, M., Tanaka-Takiguchi, Y., Hayashi, M., Nishina, M. & Goshima, G. Multiple kinesin-14 family members drive microtubule minus end-directed transport in plant cells. *J Cell Biol* **216**, 1705-1714 (2017).
10. Roberts, A.J., Kon, T., Knight, P.J., Sutoh, K. & Burgess, S.A. Functions and mechanics of dynein motor proteins. *Nature reviews. Molecular cell biology* **14**, 713-726 (2013).
11. Driskell, O.J., Mironov, A., Allan, V.J. & Woodman, P.G. Dynein is required for receptor sorting and the morphogenesis of early endosomes. *Nat Cell Biol* **9**, 113-120 (2007).
12. Jordens, I. *et al.* The Rab7 effector protein RILP controls lysosomal transport by inducing the recruitment of dynein-dynactin motors. *Current biology : CB* **11**, 1680-1685 (2001).
13. Blocker, A. *et al.* Molecular requirements for bi-directional movement of phagosomes along microtubules. *J Cell Biol* **137**, 113-129 (1997).
14. Gross, S.P. *et al.* Interactions and regulation of molecular motors in Xenopus melanophores. *J Cell Biol* **156**, 855-865 (2002).
15. Kural, C. *et al.* Kinesin and dynein move a peroxisome in vivo: a tug-of-war or coordinated movement? *Science* **308**, 1469-1472 (2005).
16. Pilling, A.D., Horiuchi, D., Lively, C.M. & Saxton, W.M. Kinesin-1 and Dynein are the primary motors for fast transport of mitochondria in Drosophila motor axons. *Mol Biol Cell* **17**, 2057-2068 (2006).
17. Gross, S.P., Welte, M.A., Block, S.M. & Wieschaus, E.F. Dynein-mediated cargo transport in vivo. A switch controls travel distance. *J Cell Biol* **148**, 945-956 (2000).
18. Bullock, S.L., Nicol, A., Gross, S.P. & Zicha, D. Guidance of bidirectional motor complexes by mRNA cargoes through control of dynein number and activity. *Current biology : CB* **16**, 1447-1452 (2006).
19. Dodding, M.P. & Way, M. Coupling viruses to dynein and kinesin-1. *The EMBO journal* **30**, 3527-3539 (2011).
20. Harrell, J.M. *et al.* Evidence for glucocorticoid receptor transport on microtubules by dynein. *The Journal of biological chemistry* **279**, 54647-54654 (2004).

21. Busson, S., Dujardin, D., Moreau, A., Dompierre, J. & De Mey, J.R. Dynein and dynactin are localized to astral microtubules and at cortical sites in mitotic epithelial cells. *Current biology : CB* **8**, 541-544 (1998).
22. Sharp, D.J., Rogers, G.C. & Scholey, J.M. Microtubule motors in mitosis. *Nature* **407**, 41-47 (2000).
23. Gaetz, J. & Kapoor, T.M. Dynein/dynactin regulate metaphase spindle length by targeting depolymerizing activities to spindle poles. *J Cell Biol* **166**, 465-471 (2004).
24. Tanenbaum, M.E., Macurek, L., Galjart, N. & Medema, R.H. Dynein, Lis1 and CLIP-170 counteract Eg5-dependent centrosome separation during bipolar spindle assembly. *The EMBO journal* **27**, 3235-3245 (2008).
25. Elting, M.W., Hueschen, C.L., Udy, D.B. & Dumont, S. Force on spindle microtubule minus ends moves chromosomes. *J Cell Biol* **206**, 245-256 (2014).
26. Heald, R. *et al.* Self-organization of microtubules into bipolar spindles around artificial chromosomes in Xenopus egg extracts. *Nature* **382**, 420-425 (1996).
27. Merdes, A., Heald, R., Samejima, K., Earnshaw, W.C. & Cleveland, D.W. Formation of spindle poles by dynein/dynactin-dependent transport of NuMA. *J Cell Biol* **149**, 851-862 (2000).
28. Quintyne, N.J., Reing, J.E., Hoffelder, D.R., Gollin, S.M. & Saunders, W.S. Spindle multipolarity is prevented by centrosomal clustering. *Science* **307**, 127-129 (2005).
29. Cheng, H.H. *et al.* Heavy chain of cytoplasmic dynein is a major component of the postsynaptic density fraction. *J Neurosci Res* **84**, 244-254 (2006).
30. Sasaki, S. *et al.* A LIS1/NUDEL/cytoplasmic dynein heavy chain complex in the developing and adult nervous system. *Neuron* **28**, 681-696 (2000).
31. Barakat-Walter, I. & Riederer, B.M. Triiodothyronine and nerve growth factor are required to induce cytoplasmic dynein expression in rat dorsal root ganglion cultures. *Brain Res Dev Brain Res* **96**, 109-119 (1996).
32. Schnapp, B.J. & Reese, T.S. Dynein is the motor for retrograde axonal transport of organelles. *Proceedings of the National Academy of Sciences of the United States of America* **86**, 1548-1552 (1989).
33. Hafezparast, M. *et al.* Mutations in dynein link motor neuron degeneration to defects in retrograde transport. *Science* **300**, 808-812 (2003).
34. El-Kadi, A.M., Soura, V. & Hafezparast, M. Defective axonal transport in motor neuron disease. *J Neurosci Res* **85**, 2557-2566 (2007).
35. Ligon, L.A., Tokito, M., Finklestein, J.M., Grossman, F.E. & Holzbaur, E.L. A direct interaction between cytoplasmic dynein and kinesin I may coordinate motor activity. *The Journal of biological chemistry* **279**, 19201-19208 (2004).
36. Chen, X.J., Xu, H., Cooper, H.M. & Liu, Y. Cytoplasmic dynein: a key player in neurodegenerative and neurodevelopmental diseases. *Science China. Life sciences* **57**, 372-377 (2014).
37. Gutierrez, P.A., Ackermann, B.E., Vershinin, M. & McKenney, R.J. Differential effects of the dynein-regulatory factor Lissencephaly-1 on processive dynein-dynactin motility. *The Journal of biological chemistry* **292**, 12245-12255 (2017).
38. Moon, H.M. & Wynshaw-Boris, A. Cytoskeleton in action: lissencephaly, a neuronal migration disorder. *Wiley interdisciplinary reviews. Developmental biology* **2**, 229-245 (2013).
39. Gerdes, J.M. & Katsanis, N. Microtubule transport defects in neurological and ciliary disease. *Cell Mol Life Sci* **62**, 1556-1570 (2005).
40. Chien, A. *et al.* Dynamics of the IFT machinery at the ciliary tip. *eLife* **6** (2017).
41. Vale, R.D. & Toyoshima, Y.Y. Rotation and translocation of microtubules in vitro induced by dyneins from Tetrahymena cilia. *Cell* **52**, 459-469 (1988).

42. Perrone, C.A. *et al.* A novel dynein light intermediate chain colocalizes with the retrograde motor for intraflagellar transport at sites of axoneme assembly in chlamydomonas and Mammalian cells. *Molecular biology of the cell* **14**, 2041-2056 (2003).
43. DeWitt, M.A., Cypranowska, C.A., Cleary, F.B., Belyy, V. & Yildiz, A. The AAA3 domain of cytoplasmic dynein acts as a switch to facilitate microtubule release. *Nature structural & molecular biology* **22**, 73-80 (2015).
44. Bhabha, G. *et al.* Allosteric communication in the dynein motor domain. *Cell* **159**, 857-868 (2014).
45. Nicholas, M.P. *et al.* Control of cytoplasmic dynein force production and processivity by its C-terminal domain. *Nature communications* **6**, 6206 (2015).
46. Kon, T., Nishiura, M., Ohkura, R., Toyoshima, Y.Y. & Sutoh, K. Distinct functions of nucleotide-binding/hydrolysis sites in the four AAA modules of cytoplasmic dynein. *Biochemistry* **43**, 11266-11274 (2004).
47. Carter, A.P., Cho, C., Jin, L. & Vale, R.D. Crystal structure of the dynein motor domain. *Science* **331**, 1159-1165 (2011).
48. Kon, T. *et al.* The 2.8 A crystal structure of the dynein motor domain. *Nature* **484**, 345-350 (2012).
49. Schmidt, H., Gleave, E.S. & Carter, A.P. Insights into dynein motor domain function from a 3.3-A crystal structure. *Nature structural & molecular biology* **19**, 492-497, S491 (2012).
50. Vallee, R.B., Williams, J.C., Varma, D. & Barnhart, L.E. Dynein: An ancient motor protein involved in multiple modes of transport. *Journal of neurobiology* **58**, 189-200 (2004).
51. Bingham, J.B., King, S.J. & Schroer, T.A. Purification of dynactin and dynein from brain tissue. *Methods in enzymology* **298**, 171-184 (1998).
52. Burgess, S.A., Walker, M.L., Sakakibara, H., Knight, P.J. & Oiwa, K. Dynein structure and power stroke. *Nature* **421**, 715-718 (2003).
53. Kon, T. *et al.* Helix sliding in the stalk coiled coil of dynein couples ATPase and microtubule binding. *Nature structural & molecular biology* **16**, 325-333 (2009).
54. Roberts, A.J. *et al.* AAA+ Ring and linker swing mechanism in the dynein motor. *Cell* **136**, 485-495 (2009).
55. Schmidt, H., Zalyte, R., Urnavicius, L. & Carter, A.P. Structure of human cytoplasmic dynein-2 primed for its power stroke. *Nature* **518**, 435-438 (2015).
56. Marzo, M.G., Griswold, J.M. & Markus, S.M. Pac1/LIS1 promotes an uninhibited conformation of dynein that coordinates its localization and activity. *biorXiv* (2019).
57. Qiu, R., Zhang, J. & Xiang, X. LIS1 regulates cargo-adapter-mediated activation of dynein by overcoming its autoinhibition in vivo. *J Cell Biol* (2019).
58. Elshenawy, M.M. *et al.* Lis1 activates dynein motility by pairing it with dynactin. *bioRxiv* (2019).
59. van Spronsen, M. *et al.* TRAK/Milton motor-adaptor proteins steer mitochondrial trafficking to axons and dendrites. *Neuron* **77**, 485-502 (2013).
60. Splinter, D. *et al.* BICD2, dynactin, and LIS1 cooperate in regulating dynein recruitment to cellular structures. *Molecular biology of the cell* **23**, 4226-4241 (2012).
61. Elshenawy, M.M. *et al.* Cargo adaptors regulate stepping and force generation of mammalian dynein-dynactin. *Nat Chem Biol* **15**, 1093-1101 (2019).
62. Kendrick, A.A. *et al.* Hook3 is a scaffold for the opposite-polarity microtubule-based motors cytoplasmic dynein-1 and KIF1C. *J Cell Biol* **218**, 2982-3001 (2019).
63. Mallik, R., Carter, B.C., Lex, S.A., King, S.J. & Gross, S.P. Cytoplasmic dynein functions as a gear in response to load. *Nature* **427**, 649-652 (2004).

64. King, S.J. & Schroer, T.A. Dynactin increases the processivity of the cytoplasmic dynein motor. *Nature cell biology* **2**, 20-24 (2000).
65. Reck-Peterson, S.L. *et al.* Single-molecule analysis of dynein processivity and stepping behavior. *Cell* **126**, 335-348 (2006).
66. Mazumdar, M., Mikami, A., Gee, M.A. & Vallee, R.B. In vitro motility from recombinant dynein heavy chain. *Proceedings of the National Academy of Sciences of the United States of America* **93**, 6552-6556 (1996).
67. Torisawa, T. *et al.* Autoinhibition and cooperative activation mechanisms of cytoplasmic dynein. *Nature cell biology* **16**, 1118-1124 (2014).
68. McKenney, R.J., Huynh, W., Tanenbaum, M.E., Bhabha, G. & Vale, R.D. Activation of cytoplasmic dynein motility by dynactin-cargo adapter complexes. *Science* **345**, 337-341 (2014).
69. Schlager, M.A., Hoang, H.T., Urnavicius, L., Bullock, S.L. & Carter, A.P. In vitro reconstitution of a highly processive recombinant human dynein complex. *The EMBO journal* **33**, 1855-1868 (2014).
70. Toba, S., Watanabe, T.M., Yamaguchi-Okimoto, L., Toyoshima, Y.Y. & Higuchi, H. Overlapping hand-over-hand mechanism of single molecular motility of cytoplasmic dynein. *Proceedings of the National Academy of Sciences of the United States of America* **103**, 5741-5745 (2006).
71. Ayloo, S. *et al.* Dynactin functions as both a dynamic tether and brake during dynein-driven motility. *Nature communications* **5**, 4807 (2014).
72. Svoboda, K., Schmidt, C.F., Schnapp, B.J. & Block, S.M. Direct observation of kinesin stepping by optical trapping interferometry. *Nature* **365**, 721-727 (1993).
73. Scharrel, L., Ma, R., Schneider, R., Julicher, F. & Diez, S. Multimotor transport in a system of active and inactive kinesin-1 motors. *Biophysical journal* **107**, 365-372 (2014).
74. Schneider, R., Korten, T., Walter, W.J. & Diez, S. Kinesin-1 motors can circumvent permanent roadblocks by side-shifting to neighboring protofilaments. *Biophysical journal* **108**, 2249-2257 (2015).
75. Mickolajczyk, K.J. *et al.* Kinetics of nucleotide-dependent structural transitions in the kinesin-1 hydrolysis cycle. *Proceedings of the National Academy of Sciences of the United States of America* **112**, E7186-E7193 (2015).
76. DeWitt, M.A., Chang, A.Y., Combs, P.A. & Yildiz, A. Cytoplasmic dynein moves through uncoordinated stepping of the AAA+ ring domains. *Science* **335**, 221-225 (2012).
77. Cleary, F.B. *et al.* Tension on the linker gates the ATP-dependent release of dynein from microtubules. *Nature communications* **5**, 4587 (2014).
78. Can, S., Dewitt, M.A. & Yildiz, A. Bidirectional helical motility of cytoplasmic dynein around microtubules. *eLife* **3**, e03205 (2014).
79. Ali, M.Y. *et al.* Myosin V is a left-handed spiral motor on the right-handed actin helix. *Nature structural biology* **9**, 464-467 (2002).
80. Brunnbauer, M. *et al.* Torque generation of kinesin motors is governed by the stability of the neck domain. *Molecular cell* **46**, 147-158 (2012).
81. Dixit, R., Ross, J.L., Goldman, Y.E. & Holzbaur, E.L. Differential Regulation of Dynein and Kinesin Motor Proteins by Tau. *Science* (2008).
82. Ferro, L.S., Can, S., Turner, M.A., ElShenawy, M.M. & Yildiz, A. Kinesin and dynein use distinct mechanisms to bypass obstacles. *eLife* **8** (2019).
83. Belyy, V., Hendel, N.L., Chien, A. & Yildiz, A. Cytoplasmic dynein transports cargos via load-sharing between the heads. *Nature communications* **5**, 5544 (2014).
84. Gennerich, A., Carter, A.P., Reck-Peterson, S.L. & Vale, R.D. Force-induced bidirectional stepping of cytoplasmic dynein. *Cell* **131**, 952-965 (2007).

85. Svoboda, K. & Block, S.M. Force and velocity measured for single kinesin molecules. *Cell* **77**, 773-784 (1994).
86. Guydosh, N.R. & Block, S.M. Direct observation of the binding state of the kinesin head to the microtubule. *Nature* **461**, 125-128 (2009).
87. Belyy, V. *et al.* The mammalian dynein-dynactin complex is a strong opponent to kinesin in a tug-of-war competition. *Nature cell biology* **18**, 1018-1024 (2016).
88. Rao, L., Berger, F., Nicholas, M.P. & Gennerich, A. Molecular mechanism of cytoplasmic dynein tension sensing. *Nature communications* **10**, 3332 (2019).
89. Nicholas, M.P. *et al.* Cytoplasmic dynein regulates its attachment to microtubules via nucleotide state-switched mechanosensing at multiple AAA domains. *Proceedings of the National Academy of Sciences of the United States of America* **112**, 6371-6376 (2015).
90. Dogan, M.Y., Can, S., Cleary, F.B., Purde, V. & Yildiz, A. Kinesin's front head is gated by the backward orientation of its neck linker. *Cell reports* **10**, 1967-1973 (2015).
91. Rai, A.K., Rai, A., Ramaiya, A.J., Jha, R. & Mallik, R. Molecular adaptations allow dynein to generate large collective forces inside cells. *Cell* **152**, 172-182 (2013).
92. Can, S., Lacey, S., Gur, M., Carter, A.P. & Yildiz, A. Directionality of dynein is controlled by the angle and length of its stalk. *Nature* **566**, 407-410 (2019).
93. Mizuno, D., Tardin, C., Schmidt, C.F. & Mackintosh, F.C. Nonequilibrium mechanics of active cytoskeletal networks. *Science* **315**, 370-373 (2007).
94. Reck-Peterson, S.L., Derr, N.D. & Stuurman, N. Imaging single molecular motor motility with total internal reflection fluorescence microscopy (TIRFM). *Cold Spring Harb Protoc* **2010**, pdb prot5399 (2010).
95. Block, S.M., Goldstein, L.S. & Schnapp, B.J. Bead movement by single kinesin molecules studied with optical tweezers. *Nature* **348**, 348-352 (1990).
96. Brangwynne, C.P., Koenderink, G.H., MacKintosh, F.C. & Weitz, D.A. Cytoplasmic diffusion: molecular motors mix it up. *J Cell Biol* **183**, 583-587 (2008).
97. Fakhri, N. *et al.* High-resolution mapping of intracellular fluctuations using carbon nanotubes. *Science* **344**, 1031-1035 (2014).
98. Forth, S., Hsia, K.C., Shimamoto, Y. & Kapoor, T.M. Asymmetric friction of nonmotor MAPs can lead to their directional motion in active microtubule networks. *Cell* **157**, 420-432 (2014).
99. Buckley, C.D. *et al.* Cell adhesion. The minimal cadherin-catenin complex binds to actin filaments under force. *Science* **346**, 1254211 (2014).
100. Huang, D.L., Bax, N.A., Buckley, C.D., Weis, W.I. & Dunn, A.R. Vinculin forms a directionally asymmetric catch bond with F-actin. *Science* **357**, 703-706 (2017).
101. Guo, B. & Guilford, W.H. Mechanics of actomyosin bonds in different nucleotide states are tuned to muscle contraction. *Proceedings of the National Academy of Sciences of the United States of America* **103**, 9844-9849 (2006).
102. Bormuth, V., Varga, V., Howard, J. & Schaffer, E. Protein friction limits diffusive and directed movements of kinesin motors on microtubules. *Science* **325**, 870-873 (2009).
103. Qiu, W. *et al.* Dynein achieves processive motion using both stochastic and coordinated stepping. *Nature structural & molecular biology* **19**, 193-200 (2012).
104. Derr, N.D. *et al.* Tug-of-war in motor protein ensembles revealed with a programmable DNA origami scaffold. *Science* **338**, 662-665 (2012).
105. Khataee, H. & Howard, J. Force Generated by Two Kinesin Motors Depends on the Load Direction and Intermolecular Coupling. *Physical review letters* **122**, 188101 (2019).
106. Feynman, R.P., Leighton, R.B. & Sands, M. *The Feynman lectures on physics, Vol. I: The new millennium edition: mainly mechanics, radiation, and heat*, Vol. 1. (Basic books, 2011).

107. Hu, D.J. *et al.* Dynein recruitment to nuclear pores activates apical nuclear migration and mitotic entry in brain progenitor cells. *Cell* **154**, 1300-1313 (2013).
108. Tan, S.C., Scherer, J. & Vallee, R.B. Recruitment of dynein to late endosomes and lysosomes through light intermediate chains. *Molecular biology of the cell* **22**, 467-477 (2011).
109. Olenick, M.A., Tokito, M., Boczkowska, M., Dominguez, R. & Holzbaur, E.L. Hook Adaptors Induce Unidirectional Processive Motility by Enhancing the Dynein-Dynactin Interaction. *The Journal of biological chemistry* **291**, 18239-18251 (2016).
110. Ori-McKenney, K.M., Xu, J., Gross, S.P. & Vallee, R.B. A cytoplasmic dynein tail mutation impairs motor processivity. *Nature cell biology* **12**, 1228-1234 (2010).
111. Gebhardt, J.C., Clemen, A.E., Jaud, J. & Rief, M. Myosin-V is a mechanical ratchet. *Proceedings of the National Academy of Sciences of the United States of America* **103**, 8680-8685 (2006).
112. Campas, O. & Sens, P. Chromosome oscillations in mitosis. *Physical review letters* **97**, 128102 (2006).
113. Pecreaux, J. *et al.* Spindle oscillations during asymmetric cell division require a threshold number of active cortical force generators. *Current biology : CB* **16**, 2111-2122 (2006).
114. Yang, G. *et al.* Architectural dynamics of the meiotic spindle revealed by single-fluorophore imaging. *Nature cell biology* **9**, 1233-1242 (2007).
115. Shingyoji, C., Higuchi, H., Yoshimura, M., Katayama, E. & Yanagida, T. Dynein arms are oscillating force generators. *Nature* **393**, 711-714 (1998).
116. Lin, J. & Nicastro, D. Asymmetric distribution and spatial switching of dynein activity generates ciliary motility. *Science* **360** (2018).
117. Laan, L. *et al.* Cortical dynein controls microtubule dynamics to generate pulling forces that position microtubule asters. *Cell* **148**, 502-514 (2012).
118. Sanchez, T., Welch, D., Nicastro, D. & Dogic, Z. Cilia-like beating of active microtubule bundles. *Science* **333**, 456-459 (2011).
119. Zhang, K. *et al.* Cryo-EM Reveals How Human Cytoplasmic Dynein Is Auto-inhibited and Activated. *Cell* **169**, 1303-1314 e1318 (2017).
120. Urnavicius, L. *et al.* Cryo-EM shows how dynactin recruits two dyneins for faster movement. *Nature* **554**, 202-206 (2018).
121. Carter, A.P. *et al.* Structure and functional role of dynein's microtubule-binding domain. *Science* **322**, 1691-1695 (2008).
122. Pyrpassopoulos, S., Shuman, H. & Ostap, E.M. Modulation of Kinesin's Load-Bearing Capacity by Force Geometry and the Microtubule Track. *Biophysical journal* **118**, 243-253 (2020).
123. Furuta, K. *et al.* Measuring collective transport by defined numbers of processive and nonprocessive kinesin motors. *Proceedings of the National Academy of Sciences of the United States of America* **110**, 501-506 (2013).
124. Brenner, S., Berger, F., Rao, L., Nicholas, M.P. & Gennerich, A. Force production of human cytoplasmic dynein is limited by its processivity. *Sci Adv* **6**, eaaz4295 (2020).
125. Andreasson, J.O. *et al.* Examining kinesin processivity within a general gating framework. *eLife* **4** (2015).
126. Gross, S.P. Hither and yon: a review of bi-directional microtubule-based transport. *Physical biology* **1**, R1-11 (2004).
127. Welte, M.A. Bidirectional transport along microtubules. *Current biology : CB* **14**, R525-537 (2004).
128. Hancock, W.O. Bidirectional cargo transport: moving beyond tug of war. *Nature reviews. Molecular cell biology* **15**, 615-628 (2014).

129. Jolly, A.L. & Gelfand, V.I. Bidirectional intracellular transport: utility and mechanism. *Biochemical Society transactions* **39**, 1126-1130 (2011).
130. Gross, S.P. Dynactin: coordinating motors with opposite inclinations. *Current biology : CB* **13**, R320-322 (2003).